THE UNIVERSITY OF MICHIGAN
COLLEGE OF ENGINEERING
Department of Meteorology and Oceanography

Technical Report

WIND VELOCITY SENSING BY MEANS OF FOUR-BLADED HELICOID PROPELLERS

Ole Christensen, Ph.D.*

administered through:
OFFICE OF RESEARCH ADMINISTRATION ANN ARBOR

December 1971

*Present affiliation:
Institute of Hydrodynamics and Hydraulic Engineering
Technical University of Denmark

Acknowledgments

This report is the partial result of one year of postdoctoral work sponsored by NATO, Brussels and the National Danish Foundation of Technical Sciences (STVF).

Some of the equipment used in the experimental work and funding to cover the costs of publication of this report were provided by ORA Project 314860, a sponsored research contract with the Detroit Edison Company.

I want to express my gratitude to all my colleagues at the Department of Meteorology and Oceanography, in particular Professors Donald J. Portman and Gerald C. Gill.

TABLE OF CONTENTS

LIST OF FIGURES

LIST OF TABLES

Introduction

In micrometeorological studies concerning either turbulent excitation of building structures or diffusion of effluents released in the surface layer of the atmosphere, there is a great demand for spatial turbulent wind measurements for scales of eddies ranging from about one meter up to several kilometers. In the past, and probably also in the years to come, this range of turbulence scales has almost exclusively been investigated by means of mechanical velocity sensors such as pitot tubes, cup anemometers, propellers, wind vanes combined with cup anemometers, and bivanes combined with propellers, to mention a few of the most typical ones. These sensors, especially the first mentioned, all share the features of being simple and sturdy, direct in their operation, and perhaps most important, they retain their calibrations well.

The cup anemometer is probably the most widely used speed sensor in the world today. It has been the subject of many investigations concerning its dynamic response. Middleton and Spilhaus (1) evaluate the more important results and offer several references. A characteristic of the cup anemometer found in many of the investigations is a significantly skewed dynamic response for accelerations and decelerations due to the unsymmetric aerodynamic shape of the cup system. Also, a cup anemometer is mounted to be sensitive to the total horizontal wind component, and a separation into longitudinal and lateral components can be done only by simultaneous operation of a wind vane (an elaboration of the sensor which does not simplify its dynamic behavior).

In their description of wind speed sensors, Middleton and Spilhaus imply that the propeller type sensor might undergo a renaissance and eventually challenge the cup anemometer in its wide use. An explanation for this possibility lies in the recent development of light materials of high strength, and in the advanced technology enabling the manufacturing of "micro-bearings" of extremely low friction. These options were not available two centuries ago when the first "windmill" sensor was suggested for registration of wind speeds. Not even a hundred years later when the first cup anemometer was described, did the propeller type sensor seem to be an alternative solution. But today, having a choice to make, it seems to be advisable to evaluate the advantages of the propeller sensor relative to those of the cup anemometer. This paper is meant to deal with some of the advantages of the propeller sensor, when the objective is to measure three-dimensional turbulent velocities in what we may call the meso-scale region.

The propeller system discussed was developed by Professor G. C. Gill of the University of Michigan in the beginning of the sixties, and is basically a four-bladed propeller, nine inches in diameter of true helicoidal shape made from polystyrene. It usually drives either a photo-chopper device or a miniature dc-tachometer generator. The propellers with photo-chopper circuits are unique in the sense that they will respond to, and provide accurate measurements of axial flow, at speeds as low as 0.2 m/s.

As the need for three-dimensional turbulence measurements became more and more apparent, Gill (2) developed a so-called "Orthogonal-UVW sensor" by mounting three propeller sensors with mutually perpendicular axes. This development resulted from the recognition that each propeller displayed a seemingly acceptable cosine response for non-axial flow. The three propellers are usually mounted with two axes horizontal and one vertical, forming an UVW coordinate system (see Figure 0.1). If, therefore, each propeller has a perfect cosine response, only the component along its axis will be registered and three-dimensional measurements may be obtained by incorporating three propellers.

Gill has long been aware of the inaccuracies in the method due to the deviation of the actual propeller response from the cosine function (see Figures 0.2-0.3). Much of his work has, therefore, been devoted to the design of propellers featuring better directional response, i.e., cosine response, but the effort has not yet resulted in any significantly better design.

In the present study, by means of a simple aerodynamic approach, we try to explore why we have a non-cosine response. At the same time the suggested model enables us to derive an expression for the dynamic response of a propeller system exposed to small velocity changes. Finally, we use the results in conducting an experimental study of the propellers' performance as directionally sensitive sensors, with the objective of designing a modified three-propeller sensor for instantaneous recording of the magnitude,

Figure 0.1

Complete UVW anemometer. By courtesy of the R. M. Young Company.

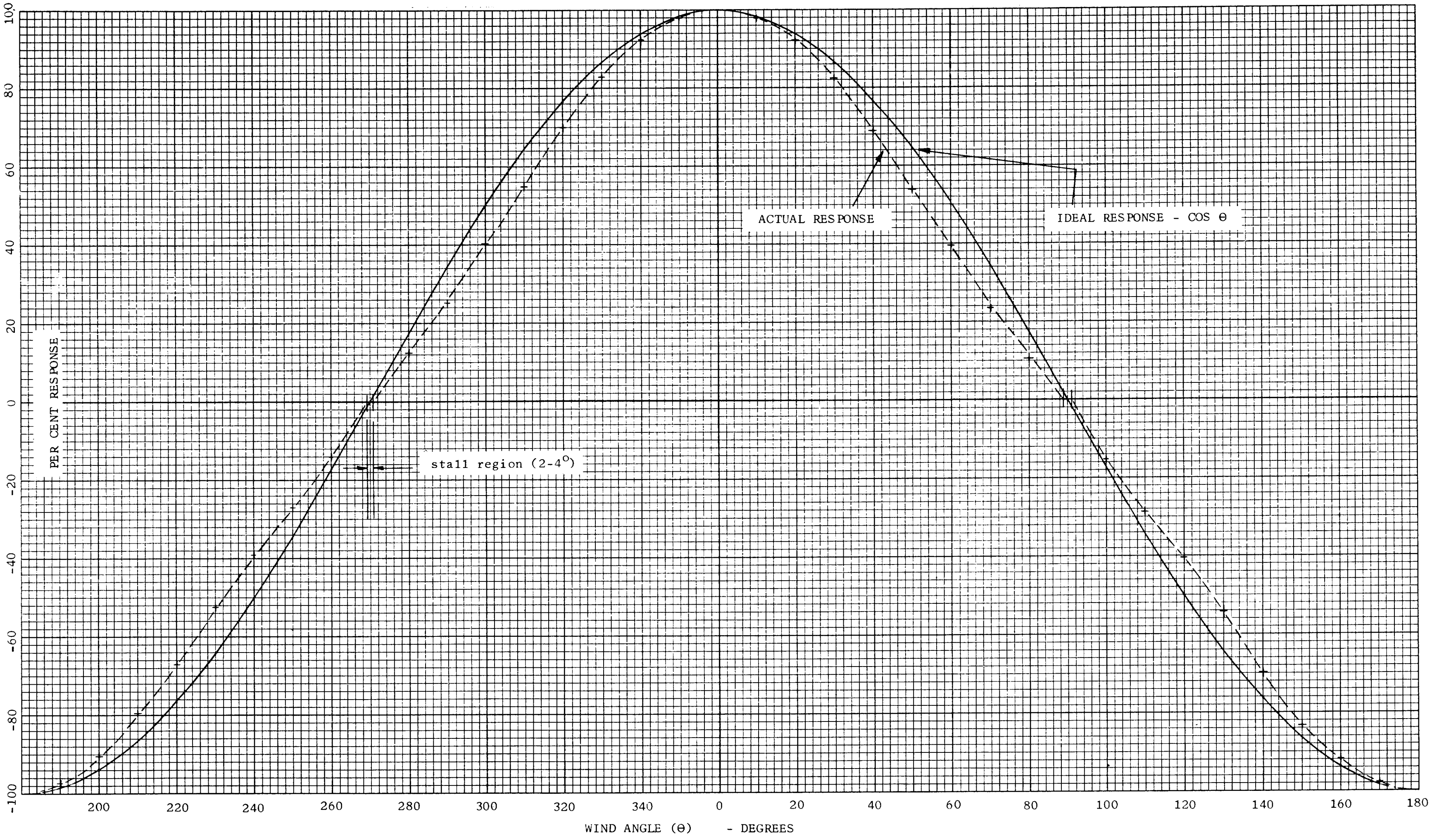

PROPELLER RESPONSE vs WIND ANGLE FOUR BLADE POLYSTYRENE PROPELLER

(data from Univ. of Mich. wind tunnel tests - May 1963)

Figure 0.2 Propeller response to non-axial flow. By courtesy of R.M. Young Company.

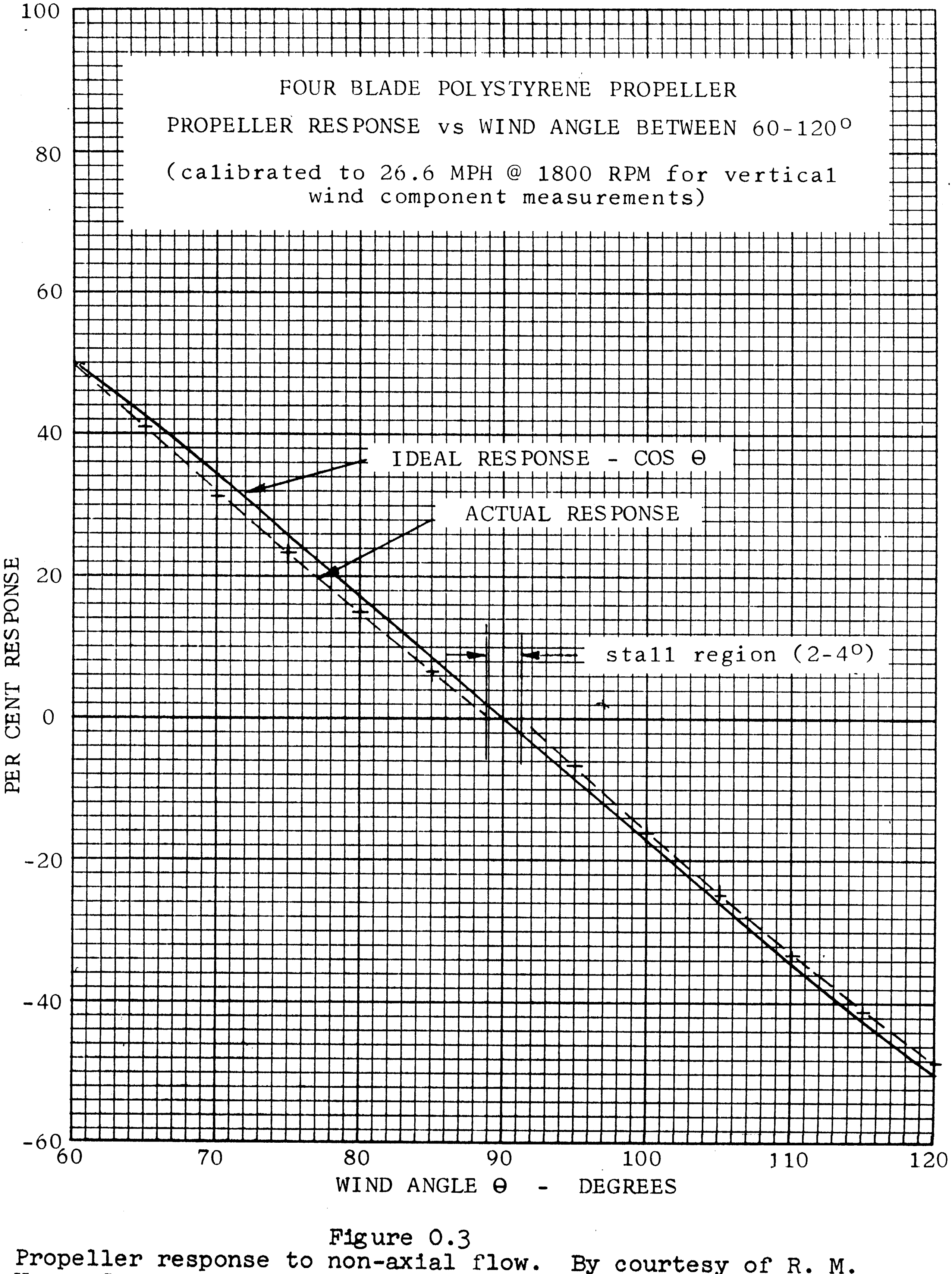

Figure 0.3
Propeller response to non-axial flow. By courtesy of R. M. Young Company

elevation and azimuth of any quasistationary wind vector, i.e., any wind vector not changing direction or magnitude faster than the propellers are able to register without any significant time lag.

1.0 An Aerodynamic Analysis of a Four-Bladed Helicoid Propeller

Due to the rotational symmetry of the helicoid propeller, we may without any loss in generality limit our analysis to a two-dimensional velocity field:

$$U_i = (U_1, U_2, 0).$$

Let us assume the propeller is mounted with its axis along the x_1-axis, yielding coincidence between the propeller plane and the x_2x_3-plane as shown in Figure 1.0.1.

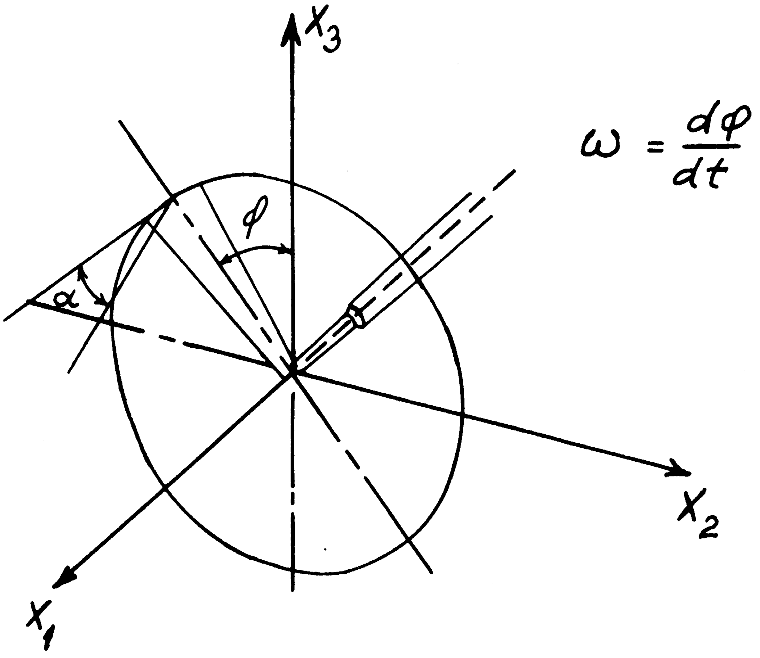

Figure 1.0.1

Reference system for the propeller motion

In the mathematical model to follow, we make certain assumptions. Some of the assumptions are of a purely mathematical nature, and they are made in order to simplify the analysis. The assumptions of a physical nature, however, are more dubious, but, in our opinion, are essential if we want to work with a mathematical model of the propeller behavior. Let us list the physical assumptions first.

Physical 1

We assume each propeller blade segment, independently of the others, to behave like an airfoil, far from the stall region, i.e., with neglectable separation occurring anywhere on the blade surface or at the blade edges.

Physical 2

We neglect any kind of friction opposing the rotation of the propeller shaft.

Ad. Physical 1

The concept of airfoil behavior of each blade segment is generally far from satisfied. But we do believe, that if we limit ourselves to relatively slowly turning propellers (γ_R large) with blade chords small ($\Delta\phi$ small) and with a small blade thickness compared to the chord ($b/a \ll 1$), we may conceive of airfoil behavior with a lift coefficient given by

$$C_L = C_L^o \cdot \epsilon \tag{1.0.1}$$

and a constant drag given by

$$C_D = \text{constant}, \tag{1.0.2}$$

where ϵ is the angle of incidence. The assumption that we work outside the stall region is closely related to the requirement that ϵ be small, which as we shall see later, implies a small U_2/U_1 ratio.

We admit that this line of thinking does not supply ready-made results concerning the response of helicoid propellers. The most evident reason for this is a lack of values for C_L^o and C_D, assuming they are constants. But, also, the fact that the obtained results logically cannot be valid for all U_2/U_1 ratios indicates that all we can expect to learn from the analysis is how the different factors involved in propeller design influence the propeller behavior when exposed to non-axial flow or when exposed to non-static axial flow. Equation (1.0.1) implies that the magnitude of the lift on the propeller blades is independent of the sign of the incidence angle. This can only be true if the blades are profiled symmetrically about an imaginative helicoidal surface having zero thickness and a pitch factor equal to the theoretical one used in the design of the propeller.

Ad. Physical 2

Obviously, one cannot conceive of bearings having zero friction. Experimental evidence indicates, however, that the bearings (and the tachometer or photochopper) used by Gill in his sensors display a cyclic frequency-dependent friction only below relatively small frequencies. At higher frequencies it becomes a constant of secondary consideration. If this holds, we might limit ourselves to not too small cyclic frequencies. Hence, a negligence of the friction term merely means a constant shift of the calibration function--cyclic frequency versus speed of axial flow--to include the origin.

We shall now turn to the necessary mathematical assumptions.

Math. 1

We assume $\Delta\phi$ small enough to allow a total geometric description of each blade segment, both as to position as well as to shape, and to depend upon:

a) radius vector r

b) pitch angle $\alpha(r)$

c) ϕ

d) chord length $a(r)$

e) blade thickness $b(r)$

In other words, we consider each blade segment as a geometrical unit fully described by r and functions of r.

Math. 2

We assume

$$U_2/U_R << \frac{(\omega/\omega_R)^2 + (R\gamma_R/r)^2 \cdot (U_1/U_R)^2}{(\omega/\omega_R) \cdot R\gamma_R/r} \, . \qquad (1.0.3)$$

This assumption is necessary partly to fulfill Physical 1 and partly to allow mathematical linearizing.

Math. 3

ϵ is assumed small enough to allow mutual substitutions between ϵ and $\tan \epsilon$.

Math. 4

We assume $R_o/R \ll 1$, and hence neglect the effect of R_o.

Ad. Math 1

Consequences of small $\Delta\phi$ are that

$$\tan \alpha = \gamma_R R/r \tag{1.0.4}$$

and

$$a = \Delta\phi r \sqrt{1 + (\gamma_R R/r)^2} , \tag{1.0.5}$$

and if we only allow linearly changing blade thickness, we may add

$$b = b_1 (1 - (1 - b_2/b_1) r/R). \tag{1.0.6}$$

The derivation of Equation (1.0.4) becomes intuitive by a glance at Figure 1.0.2.

Ad. Math 2

Equation (1.0.3) is not at all obvious at the present time; we therefore only mention its existence for the benefit of clarity. We may for a moment look upon the consequences of Equation

(1.0.3). A result to be discussed later (Equation (1.1.11)) yields $k\omega/\omega_R = U_1/U_R$. Hence, putting $\gamma_R\, R/r \simeq \gamma_R$ results in

$$U_2 \ll U_1 \; \frac{1 + \gamma_R^{\,2}}{\gamma_R^{\,2}} \; .$$

If, for example, $\gamma_R = 0.5$, which is a reasonable value, we obtain $U_2 \ll 5U_1$. Since the lateral component in a turbulent flow seldom exceeds 50 percent of the longitudinal component, we can expect Equation (1.0.3) to be valid. Thus, for a propeller axially aligned parallel to the mean flow, Equation (1.0.3) expresses an acceptable assumption if the objective is the recording of low frequencies of turbulence.

Ad. Math 3

Figure 1.0.2 shows a top view of a blade segment, and the relevant velocity vectors.

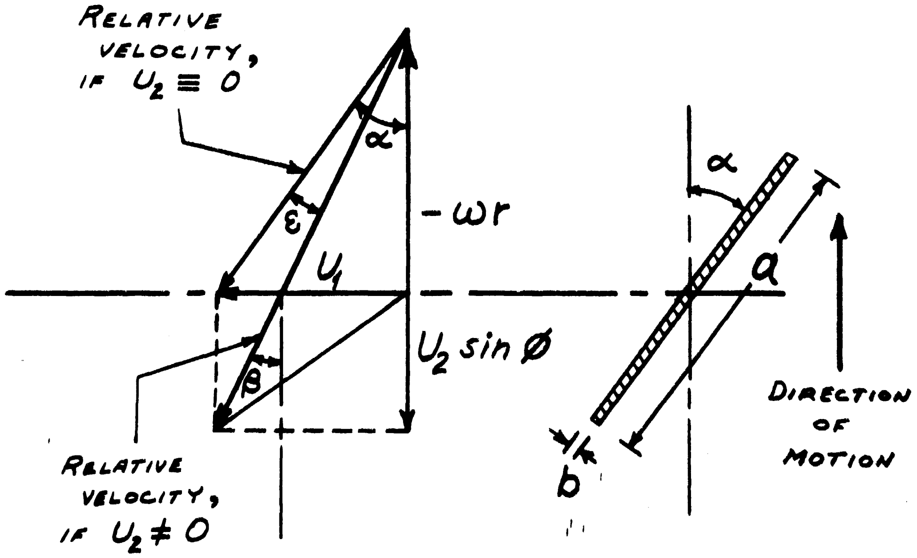

Figure 1.0.2

Vector diagram of velocities relative to a blade cross-section

From Figure 1.0.2, we can see that

$$\tan\beta = \frac{U_1}{\omega r + U_2 \sin\phi}\ , \qquad (1.0.7)$$

and since $\epsilon = \beta - \alpha$ we obtain

$$\epsilon = \tan^{-1} \frac{\gamma_R (U_1/U_R - \omega/\omega_R) - \gamma_R^{\,2}\ U_1/U_R \sin\phi}{\gamma_R\ U_1/U_R \sin\phi + \omega/\omega_R\ r/R + \gamma_R^{\,2}\ U_1/U_R\ R/r}\ . \qquad (1.0.8)$$

Equations (1.0.8) and (1.0.3) indicate that Math. 3 is fulfilled if $(U_1/U_R - \omega/\omega_R)$ is small.

We are now ready to write down the equation of motion for the propeller. We obtain

$$I \cdot d^2\phi/dt^2 - M\ (U_1/U_R,\ U_2/U_R,\ 1/\omega_R\ d\phi/dt,\ \phi) = 0, \qquad (1.0.9)$$

where I denotes the moment of inertia of the propeller about its axis and M denotes the momentum of forces acting on the blade surfaces about the same axis.

If index i symbolizes blade number i, we may write

$$M = \sum_{i=1}^{4} \int_0^1 \tfrac{1}{2}\rho_a\ V_i^2\ a\ R^2\ (C_L^o\ \epsilon_i\ \sin\beta_i - C_D \cos\beta_i)\ d(r/R), \qquad (1.0.10)$$

where under the assumptions made we have

$$V_i \simeq U_R \sqrt{(\omega/\omega_R)^2 + (\gamma_R\ R/r)^2\ (U_1/U_R)^2}$$

$$\cdot \left\{ 1 + \frac{(\gamma_R\ R/r) U_2/U_R\ \omega/\omega_R\ \sin\phi_i}{(\omega/\omega_R)^2 + (\gamma_R\ R/r)^2 (U_1/U_R)^2} \right\},$$

$$\mathrm{Sin}\beta_i \simeq \frac{\gamma_R\ R/r\ U_1/U_R}{((\omega/\omega_R)^2 + (\gamma_R\ R/r)^2\ (U_1/U_R)^2)^{\frac{1}{2}}}$$

$$\cdot \left\{ 1 - \frac{(\gamma_R\ R/r)\ U_2/U_R\ \omega/\omega_R\ \sin\phi_i}{(\omega/\omega_R)^2 + (\gamma_R\ R/r)^2 (U_1/U_R)^2} \right\},$$

$$\epsilon_i \simeq \frac{(U_1/U_R - \omega/\omega_R) - (\gamma_R R/r)\ U_2/U_R\ \sin\phi_i}{U_2/U_R\ \sin\phi_i + (r/R/\gamma_R)\ (\omega/\omega_R + (\gamma_R R/r)^2\ U_1/U_R)},$$

and, finally,

$$\cos\beta_i \simeq \frac{\omega/\omega_R}{((\omega/\omega_R)^2 + (\gamma_R R/r)^2\ (U_1/U_R)^2)^{\frac{1}{2}}}$$

$$\cdot \left\{ 1 + \frac{(\gamma_R R/r)\ U_2/U_R\ (U_1/U_R)^2\ \omega_R/\omega}{(\omega/\omega_R)^2 + (\gamma_R R/r)^2\ (U_1/U_R)^2} \right\}.$$

By working with two opposing blades at a time, and adding together their respective contributions to the total momentum of forces, we obtain after some laborious but simple reductions

$$M = \rho_a \; U_R{}^2 \; R^2 \cdot \int_0^1 a(r/R) \cdot \sqrt{(\omega/\omega_R)^2 + (\gamma_R R/r \; U_1/U_R)^2} \tag{1.0.11}$$

$$\cdot \left\{ U_1/U_R \cdot (U_1/U_R - \omega/\omega_R) \cdot \frac{\text{LFN } (\omega/\omega_R,\; U_1/U_R,\; U_2/U_R, \phi,\; r/R)}{\text{LFD } (\omega/\omega_R,\; U_1/U_R,\; U_2/U_R, \phi,\; r/R} \; C_L^o \right.$$

$$\left. - \frac{\text{DGN } (\omega/\omega_R,\; U_1/U_R,\; U_2/U_R, \phi,\; r/R)}{\text{DGD } (\omega/\omega_R,\; U_1/U_R,\; U_2/U_R, \phi,\; r/R)} \cdot C_D \right\} d(r/R) .$$

The following substitutions have been made into Equation (1.0.11):

$$\text{LFN} = \tag{1.0.12}$$

$$2 \left\{ (\omega/\omega_R)^3 + (\gamma_R R/r)^2 \; \omega/\omega_R \; U_1/U_R \; (\omega/\omega_R + U_1/U_R) \right\}$$

$$\cdot \left\{ \omega/\omega_R + (\gamma_R R/r)^2 \; U_1/U_R \right\}^2$$

$$+ \quad (\gamma_R R/r)^2 \; (U_2/U_R)^2 \; \left\{ (\gamma_R R/r)^6 \; (U_1/U_R)^3 + 2 \; (\gamma_R R/r)^4 \right.$$

$$\cdot \; (U_1/U_R)^2 \; \omega/\omega_R - (\gamma_R R/r)^2 \; U_1/U_R \; \omega/\omega_R \; (2\omega/\omega_R + U_1/U_R)$$

$$\left. - \; 2 \; (\omega/\omega_R)^3 \right\}$$

$$+ \quad (\gamma_R R/r)^4 \; (U_2/U_R)^4 \; \left\{ (\gamma_R R/r)^2 \; (U_1/U_R) - \omega/\omega_R \right\} \cdot \tfrac{1}{2} \sin^2 2\phi ,$$

LFD = (1.0.13)

$$\left\{(\omega/\omega_R)^2 + (\gamma_R R/r)^2 (U_1/U_R)^2\right\} \cdot \left\{(\omega/\omega_R) + (\gamma_R R/r)^2 U_1/U_R)\right\}^4$$

$$- \left\{(\omega/\omega_R) + (\gamma_R R/r)^2 (U_1/U_R)\right\}^2 \cdot (\gamma_R R/r)^2 (U_2/U_R)^2$$

$$+ (\gamma_R R/r)^4 (U_2/U_R)^4 \cdot \tfrac{1}{2} \sin^2 2\phi ,$$

DGN = (1.0.14)

$$2 (\omega/\omega_R)^3 + (\gamma_R R/r)^2 (U_2/U_R)^2 (\omega/\omega_R) ,$$

and

DGD = (1.0.15)

$$(\omega/\omega_R)^2 + (\gamma_R R/r)^2 (U_1/U_R)^2 .$$

If we now recall Equation (1.0.3), we notice that the ϕ dependence of the functions FFD and LFN is small (of the order of $(U_2/U_R)^4$). Hence, we may conclude that M does not depend significantly upon ϕ, which implies that the equation of motion can be reduced to a first order differential equation in ω/ω_R.

Due to the complexity of Equation (1.0.11), we cannot obtain an analytical solution to Equation (1.0.9). It therefore becomes necessary to continue the analysis in two parts: one part in a form to reveal features of the equilibrium solution to non-axial flow, and the second part in a form concerned with the dynamic response of the propeller to small changes in axial flow.

1.1 Directional Sensitivity: Angular Response Function

Equilibrium solutions to the equation of motion (Equation (1.0.9)) are obtained by

$$M = 0. \tag{1.1.1}$$

This is true only because of M's approximate independence of ϕ.

The angular response function is defined by

$$S(\theta) = \omega/\omega_\infty, \tag{1.1.2}$$

where ω_∞ is the equilibrium cyclic frequency of axial flow of strength U. ω is the cyclic frequency obtained at equilibrium for non-axial flow of the same strength, but at a slope toward the propeller plane of $\cot\theta$.

By introducing Equation (1.1.2) and a polar notation for the velocity vector $(U_1, U_2, 0)$ into Equations (1.0.12) through (1.0.15) we obtain

$$\text{LFN} = \tag{1.1.3}$$

$$2\left\{(\omega_\infty/\omega_R)^3\ S^3 + (\gamma_R R/r)^2\ (\omega_\infty/\omega_R)\ (U/U_R)\ S\cos\theta \cdot (\omega_\infty/\omega_R\ S + U/U_R\ \cos\theta)\right\}\left\{S\ \omega_\infty/\omega_R + (\gamma_R R/r)^2 \cdot U/U_R\ \cos\theta\right\}^2$$

$$+ \quad (\gamma_R R/r)^4 \; (U/U_R)^4 \; \sin^2\theta \; \cos^2\theta \; \Big\{(\gamma_R R/r)^4 \; (U/U_R) \; \cos\theta$$

$$+ \; \omega_\infty/\omega_R \; S \; (2(\gamma_R R/r)^2 + 1)\Big\} \; ,$$

$$\text{LFD} = \tag{1.1.4}$$

$$\Big\{(\omega_\infty/\omega_R)^2 \; S^2 + (\gamma_R R/r)^2 \; (U/U_R)^2 \; \cos^2\theta\Big\}\Big\{\omega_\infty/\omega_R \; S$$

$$+ \; (\gamma_R R/r)^2 \; U/U_R \; \cos\theta\Big\}^4 ,$$

$$\text{DGN} = \tag{1.1.5}$$

$$2 \; (\omega_\infty/\omega_R)^3 \; S^3 + (\gamma_R R/r)^2 \; (U/U_R)^2 \; \sin^2\theta \; \omega_\infty/\omega_R \; S \; ,$$

and

$$\text{DGD} = \tag{1.1.6}$$

$$(\omega_\infty/\omega_R)^2 \; S^2 + (\gamma_R R/r)^2 \; (U/U_R)^2 \; \cos^2\theta \; .$$

According to the theorem of "Integral Mean Value" it is possible to determine a number δ lying in the interval

$$0 \leq \delta \leq 1/\gamma_R ,$$

for which we may write

$$\begin{aligned} M = {} & \rho_a \Delta\phi \, U_R^2 \, R^3 \, \gamma_R \sqrt{\delta^2 + 1} \cdot \sqrt{(\omega_\infty/\omega_R)^2 \, S^2 + (U/U_R)^2 \cos^2\theta/\delta^2} \qquad (1.1.7) \\ & \cdot \{ U/U_R \cos\theta \, \{ U/U_R \cos\theta - \omega_\infty/\omega_R \cdot S \} \\ & \cdot \frac{\mathrm{LFN}\ (S,\ \omega_\infty/\omega_R,\ U/U_R, \theta, \delta)}{\mathrm{LFD}\ (S,\ \omega_\infty/\omega_R,\ U/U_R, \theta, \delta)} \cdot C_L^o - \frac{\mathrm{DGN}\ (S,\ \omega_\infty/\omega_R,\ U/U_R, \theta, \delta)}{\mathrm{DGD}\ (S,\ \omega_\infty/\omega_R,\ U/U_R, \theta, \delta)} \, C_D \} . \end{aligned}$$

Equation (1.1.1) together with Equation (1.1.7) yield the basis for determining the form of the propeller calibration function

$$\omega/\omega_R = F\ (U/U_R, \theta). \qquad (1.1.8)$$

Let us first consider the imaginative case that $C_D = 0$. In this case--and this case only--M = 0 if

$$U/U_R \cos\theta = \omega_\infty/\omega_R \cdot S,$$

or rewritten in the form of Equation (1.1.8),

$$\omega/\omega_R = U/U_R \cos\theta. \qquad (1.1.9)$$

Equation (1.1.9) means that the propeller displays a perfect cosine response to non-axial flow.

In reality, however, C_D is not zero, although C_D/C_L^o is expected to be small (somewhere between 0.1 and 0.01). But due to the way Equation (1.1.7) is composed, the effect of even a small C_D/C_L^o may be significant, depending upon the magnitude of the coefficients to C_L^o and C_D. Knowing that these coefficients are positive we conclude

$$U/U_R \cos\theta \geq \omega_\infty/\omega_R \cdot S, \qquad (1.1.10)$$

for all θ of which Equation (1.1.7) is valid. If we therefore define

$$k \cdot \omega_\infty/\omega_R = U/U_R \qquad (1.1.11)$$

and substitute Equation (1.1.10) together with $\theta = 0$, into the expression for M, we obtain by means of Equation (1.1.1)

$$C_D/C_L^o = \frac{1 + 1/\delta^2 k}{1 + k + 1/\delta^4 k^2} \; k \; (k - 1). \qquad (1.1.12)$$

This expression indicates, however, that $k > 1$. Hence, $k = 1 + \Delta$ for $\Delta^2 << 1$ yields

$$k \simeq 1 + \frac{2\delta^4 + 1}{\delta^2(\delta^2 + 1)} \; C_D/C_L^o, \qquad (1.1.13)$$

if, which is very likely, δ is of the order of unity.

Introducing the pitchfactor $\gamma_R = U_R/(R\omega_R)$ into Equation (1.1.11), we obtain

$$U/R\cdot\omega = k\cdot\gamma_R = \gamma_T \ . \qquad (1.1.14)$$

Hence, the drag coefficient effectively increases the propeller pitchfactor by a factor approximately C_D/C_L^o greater than one. (Usually this does not have any practical significance, being only an increase of a few percent.)

Let us summarize the above discussion of the equilibrium behavior of the propeller exposed to non-axial flow. The calibration function may be expressed as

$$(R\cdot\omega)\cdot\gamma_T = S\cdot U, \qquad (1.1.15)$$

where $\gamma_T = k\cdot\gamma_R$, $k > 1$. k is a function entirely of γ_R and C_D/C_L^o; while S is a function of γ_R, θ, and C_D/C_L^o only.

Concerning the form of S, we have only obtained limited knowledge, namely that

$S(0) = 1$ by definition, and

$\frac{S(\theta)}{\cos\theta} < k$ for all θ within our basic assumptions.

1.2 Dynamic Response to Small Changes in Axial Flow

In order to formulate an analytical solution to Equation (1.0.9), we have to expand our basic mathematical assumptions and limit ourselves to cases of small amplitude changes in the velocity field approaching the propeller. Furthermore, we shall only attempt to solve the equation of motion in the special case of axial flow ($\theta = 0$), suddenly changed from one state of equilibrium to another state of equilibrium.

We prescribe:

$$U(t) = U_o; \quad t < 0$$

and $\qquad$ (1.2.1)

$$U(t) = (1 + p)\, U_o; \; t \geq 0; \; |p| \ll 1.$$

By defining

$$\Omega(t) = 1/k \cdot \omega(t)/\omega_\infty, \tag{1.2.2}$$

we know from Chapter 1.1 that

$$k\, \omega_\infty/\omega_R = (1 + p)\, U_o/U_R. \tag{1.2.3}$$

Hence,

$$\omega(t)/\omega_R = \Omega(t) \cdot (1 + p)\, U_o/U_R . \qquad (1.2.4)$$

The limitation on p and our knowledge from Chapter 1.1 concerning k allow us to put $\Omega(t) = 1 - \omega'$, and to disregard second and higher order terms of ω'.

From Equation (1.0.11) we thus obtain

$$dM = 2\rho_a \cdot \Delta\phi \cdot \gamma_R{}^2\, R^3 \left\{(1 + p)\, U_o\right\}^2 \cdot \left\{C_L^o dIN_1 - C_D dIN_2\right\}, \qquad (1.2.5)$$

where

$$dIN_1 \simeq + \omega' \frac{x^5 + 2x^3}{(x^2 + 1)^2}\, dx$$

and

$$dIN_2 \simeq x - \omega'\, x/1 + x^2 \;\; dx,$$

while

$$x = \Omega(t)\, r/\gamma_R \cdot R .$$

An integration of Equation (1.2.5) over the interval $(0 \leq x \leq \Omega/\gamma_R)$, and a final linearizing with respect to ω' yield

$$M = \rho_a \, \Delta\phi \left\{(1 + p) \, U_o\right\}^2 R^3 \left\{C_L^o \cdot G\,(\gamma_R, \, C_D/C_L^o) \, \omega' - C_D\right\}, \qquad (1.2.6)$$

where

$$G(\gamma_R, C_D/C_L^o) = \frac{1+C_D/C_L^o \; (2+\gamma_R^2(2+\ln((1+\gamma_R^2)/\gamma_R)) + \gamma_R^4 \ln((1+\gamma_R^2)/\gamma_R^2)}{1 + \gamma_R^2} . (1.2.7)$$

The moment of inertia of the propeller may be estimated by

$$I = 4\rho_m \, R^3 \int_0^1 b(r/R) \cdot a(r/R) \cdot (r/R)^2 \cdot d(r/R). \qquad (1.2.8)$$

Performing the integration yields

$$I = \rho_m \, b_1 \, R^4 \, \Delta\phi \, (I_1(\gamma_R) + b_2/b_1 \, I_2(\gamma_R)), \qquad (1.2.9)$$

where

$$I_1(\gamma_R) = 1/30 \, \Big\{(16\gamma_R^4 + 7\gamma_R^2 + 6)\sqrt{\gamma_R^2 + 1} - (16\gamma_R^5 + 15\gamma_R^4$$

$$\cdot \ln\,(1 + \sqrt{\gamma_R^2 + 1/\gamma_R})\Big\}, \text{ and} \qquad (1.2.10)$$

$$I_2(\gamma_R) = 1/15 \, \left\{8\gamma_R^5 - (8\gamma_R^4 - 4\gamma_R^2 - 12) \sqrt{1 + \gamma_R^2}\right\}. \qquad (1.2.11)$$

Substitution of Equations (1.2.9), (1.2.6) and (1.2.2) into the equation of motion (Equation (1.0.9)) yields

$$\frac{d\omega}{dt} + \frac{\rho_a \cdot \gamma_R \cdot (1+p)\ U_o \cdot C_L^o \cdot G(\gamma_R,\ C_D/C_L^o)}{\rho_m\ b_1\ (I_1(\gamma_R) + b_2/b_1\ I_2(\gamma_R))} \cdot \omega'$$

$$- \frac{\rho_a\ \gamma_R\ (1+p)\ U_o \cdot C_D}{\rho_m\ b_1\ (I_1(\gamma_R) + b_2/b_1 I_2(\gamma_R))} = 0\ . \qquad (1.2.12)$$

Introducing

$$T^{-1} = \frac{(1+p)\ U_o}{L} = \frac{\rho_a \cdot \gamma_R \cdot (1+p)\ U_o\ C_L^o \cdot G}{\rho_m\ b_1\ (I_1 + b_2/b_1\ I_2)} \qquad (1.2.13)$$

and

$$\omega_o'/T = \frac{\rho_a\ \gamma_R\ (1+p)\ U_o\ C_D}{\rho_m\ b_1 (I_1 + b_2/b_1 I_2)}\ , \qquad (1.2.14)$$

we have

$$\frac{d(\omega_o' - \omega')}{dt/T} + (\omega_o' - \omega') = 0. \qquad (1.2.15)$$

The initial condition, for the particular solution to Equation (1.2.15) we are looking for, can be derived from Equations (1.2.1), (1.2.3), and (1.2.4). We obtain

$$\omega'(t = 0) = 1 - 1/k(1+p).$$

Hence the solution is

$$\omega'(t) = \omega_o' + (1 - \omega_o' - 1/k(1+p))\, e^{-t/T},$$

or, by means of $\Omega(t) = 1 - \omega'(t)$,

$$\Omega(t) = 1 - \omega_o' - (1 - \omega_o' - 1/k(1+p))\, e^{-t/T}. \qquad (1.2.16)$$

For t approaching infinity,

$$k = 1/(1 - \omega_o'). \qquad (1.2.17)$$

Equations (1.2.2), (1.2.16) and (1.2.17) finally yield

$$\omega(t)/\omega_\infty = 1 - (1 - 1/(1+p))e^{-t/T} \simeq 1 - pe^{-t/T}. \qquad (1.2.18)$$

Equation (1.2.18) indicates that for small changes in axial flow ($|p| \ll 1$), the discussed helicoid propeller displays first order response. Furthermore, the distance constant L is unchanged from an acceleration response ($p > 0$) to a deceleration response ($p < 0$).

The distance constant is given by

$$L = \frac{\rho_m \, b_1 \, (I_1(\gamma_R) + b_2/b_1 I_2(\gamma_R))}{\rho_a \, \gamma_R \, C_L^o \cdot G(\gamma_R, \, C_D/C_L^o)}, \qquad (1.2.19)$$

where $G(\gamma_R, C_D/C_L^o)$ is defined by Equation (1.2.7), $I_1(\gamma_R)$ by Equation (1.2.10), and $I_2(\gamma_R)$ by Equation (1.2.11).

The offset, ω_o', due to the drag coefficient, C_D, is given by

$$\omega_o' = 1/G(\gamma_R, \, C_D/C_L^o) \cdot C_D/C_L^o \, . \qquad (1.2.20)$$

G, being of the order of unity, sustains our earlier finding that k is only a few percent larger than unity; a necessary property for the above outlined deductions concerning the dynamic propeller response.

2.0 An Experimental Study of Propeller Performance to Axial and to Non-Axial Flow

A way of mounting helicoid propellers for three-dimensional turbulence measurements is the three-propeller array suggested by Gill (2). The major advantage of this system is that continuous recordings can be made despite changes in mean wind direction, a convenience which is partially offset by diminished accuracy of the statistical estimates of the flow properties in the vicinity of the propeller array. Most of the inaccuracy is due to the propellers' lack of perfect cosine response to non-axial flow. This source of inaccuracy, however, may be diminished substantially by means of correction terms relating the actual direction response of the propellers to a pure cosine response.

A more serious source of inaccuracy concerns the vertical propeller. Usually the fluid under study is a horizontal mean wind with three-dimensional turbulent fluctuations. Hence, the propeller measuring fluctuations in the vertical wind component must reverse direction of rotation sufficiently often to yield a zero mean reading. Wind tunnel tests indicate, however, a threshold region of attack angles for which the propeller does not turn at all. Depending upon friction, this region is approximately $\pm 2^{\circ}$ from the horizontal plane. If the horizontal wind component is sufficiently large, the instantaneous wind vector within this threshold region may have a significant vertical component. For this condition, a source of error exists that cannot easily be eliminated. We therefore pose the question: can more accurate measurements be achieved by simply changing the orientation of the three propellers? The answer, we believe, is yes, if we accept a more elaborate setup with possible changes of alignment during recording, and if we have access to a digital computer of reasonable size. The basic idea behind such a system is to orient the three propellers in such a manner that the instantaneous wind vector at no time reverses the direction of revolution of any of the propellers. The wind vector will thus at any time be determinable, in magnitude as well as in position, by means of the three instantaneous rates of revolution of the propellers. The accuracy in determination of the wind vector is entirely dependent upon our knowledge of the propeller response to changing non-axial flows.

Guided by the results of Chapter 1 we undertook an experimental study with the goal of developing a mathematical formula for the propeller response. In the experimental setup it was impossible to investigate the dynamic response function of the propeller system. In the following, we assume equivalence between the static and the dynamic response function. This assumption may in general be questioned, but there can be little doubt of its validity if the rate of flow change is small enough to insure zero lag between the instantaneous flow rate and the equivalent propeller revolution rate.

The experiments are divided into two parts. Part one (Chapter 2) deals with the directional calibration of helicoid propellers and an attempt to verify the equation for calibration (obtained in Chapter 1), together with its limitations. Part two (Chapter 3) is designed to evaluate the inaccuracies expected in three-dimensional velocity measurements made with an array of three propellers and the calibration formulas obtained in part one.

2.1.0 Calibration

The experimental study was performed on two types of four-bladed helicoid propellers. The geometric and physical properties of the propellers are listed in Table 2.1.1. The pitchfactor γ_R is defined as the magnitude of the axial flow that theoretically yields a blade tip velocity of unity under a no-slip condition.

Propeller Type and diameter	R_i m	R m	$\Delta\phi$ rad.	b_1 m	b_2 m	γ_R	ρ_m Kg/m^3
20 cm Aluminum	.008	.100	.628	.0076	.0028	.477	2940
9" Polystyrene	.008	.114	.611	.0005	.0005	.424	100

Table 2.1.1
Geometrical and physical properties of propellers

The work was carried out partly in the low speed open circuit wind tunnel belonging to the Department of Meteorology and Oceanography, and partly in the subsonic closed circuit wind tunnel belonging to the Department of Aerospace Engineering; both are part of the College of Engineering at the University of Michigan. The MO tunnel has a cross section of 2 x 3 ft in its test section, and any wind speed between zero and approximately 12 m/s can be obtained with a high degree of stability. The AE tunnel has a cross section of 5 x 7 ft and may be operated at any speed below approximately 90 m/s.

The performance of the aluminum propeller was only investigated in the MO tunnel at five speeds below 12 m/s while the polystyrene propellers were tested at speeds ranging from about 1 m/s to 25 m/s. 25 m/s is slightly above the upper range limit specified by the manufacturer.

The measuring procedure was as follows. The propeller probe--i.e., propeller mounted on a stainless steel shaft and driving a photo-chopper transducer--was set up in the test section on a special machanical device enabling us to measure the angle between the tunnel axis and the propeller axis (see Figures 2.1.1 and 2.1.2). At a given tunnel speed, and by means of an electronic counter, we measured the speed of revolution of the propeller versus different flow angles of attack. The tunnel speed was then changed and a new series of measurements of speed of rotation versus angle of attack were made. The tunnel speed was measured by means of a pitot tube and a precision manometer. Since a pitot tube measurement is not very accurate at very low speeds (less then 4 m/s) a separate propeller anemometer was used as a reference propeller in some of the calibrations.

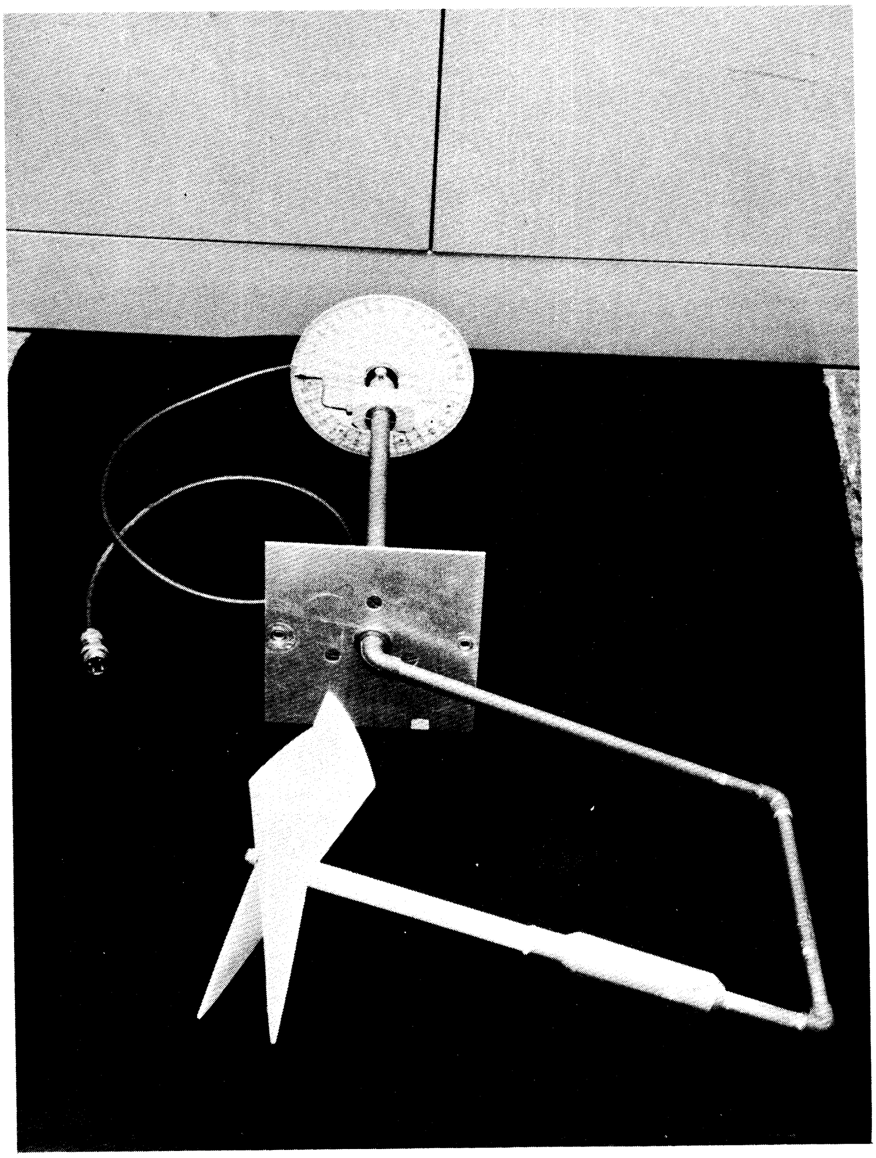

Figure 2.1.1

Mounting device for measurement of propeller response to non-axial flow.

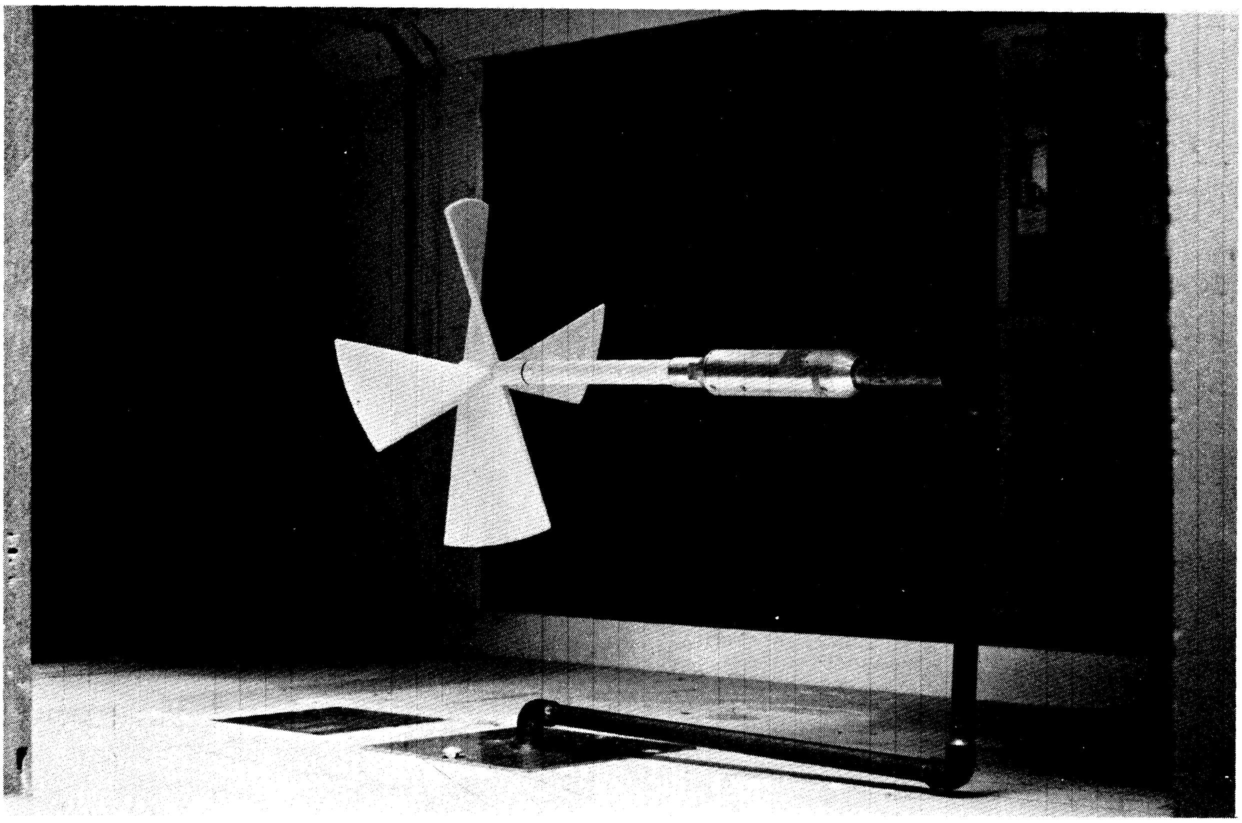

Figure 2.1.2
Propeller mounted in the MO wind tunnel.

2.1.1 Calibration for Axial Flow

From Chapter 1 of this report we learn that the expected calibration function may be written as

$$\gamma_T R\omega = S(\theta)\cdot(U - \Delta U), \qquad (2.1.1)$$

where $\gamma_T = k\gamma_R$ is the actual propeller pitchfactor that theoretically should be a few percent larger than the "mathematical" pitchfactor, γ_R. $S(\theta)$, the angular response function for the propeller, is unity for $\theta = 0$, and $\cos\theta - S(\theta) > 0$ for values of θ close to zero.

Table 2.1.2 gives a summary of the obtained calibration results for $\theta = 0$. In the table we have used the values of γ_R from Table 2.1.1.

The magnitude of the standard deviations of γ_T and ΔU indicate the validity of Equation (2.1.1) for $\theta = 0$. A mutual comparison among the obtained γ_T values for the different polystyrene propellers indicates, however, some rather large differences in response. The runs marked with an asterisk in column two show a considerable deviation from the rest. Some of these differences may have been introduced by an unknown experimental bias (three runs were performed about three months earlier than the rest). On the other hand, the measuring procedure has been so carefully checked that it is hard to believe the whole difference (about 5 percent) has been caused by experimental

Propeller		Calibration Specifications				Results from Regression				
Type	Identifier	Range min $^{m}/_{s}$	Range max $^{m}/_{s}$	No. of points	Ambient temp. $^{\circ}C$	γ_T	S.D. γ_T	U m/s	S.D. ΔU m/s	$\frac{\gamma_T - \gamma_R}{\gamma_R}$ x 100%
Aluminum O.D. .200 m	A	1.25	11.34	5	21	.470	.008	.15	.02	-1.5
Polystyrene O.D. .228 m	Q*	1.01	9.47	3	17	.443		.00		4.5
	U*	5.00	26.12	5	16	.444	.002	-.27	.02	4.6
	do	.70	11.23	7	30	.428	.001	.004	.003	1.0
	do	2.08	11.26	6	31	.428	.005	.01	.02	1.0
	V*	5.00	26.12	5	16	.439	.003	-.25	.03	3.5
	do	2.08	11.26	6	31	.427	.005	.01	.02	.7
	W	2.08	11.26	6	31	.425	.006	.01	.02	.2
	Ref	1.48	11.26	7	27	.424	.001	.004	.005	.0
	do	2.08	11.26	6	31	.424	.005	.01	.02	.0
	X	1.48	11.26	7	27	.419	.001	.014	.003	-1.1
	Y	1.48	11.26	7	27	.420	.001	.011	.005	- .9
	Z	5.49	11.26	5	27	.423	.001	.025	.005	- .2

Table 2.1.2

Calibration specifications for aluminum and polystyrene propellers for axial flow ($\theta = 0$)

errors. Hence, if we view the information in Table 2.1.2 as unbiased results, we notice a significant difference in ambient temperature between runs displaying large differences of γ_T. The results indicate about one percent increase in propeller speed per 5°C increase in ambient temperature. This result cannot be regarded as conclusive unless experimental evidence is found to support it (see Appendix B). The last column in Table 2.1.2 seems to indicate a disagreement with the theoretical result $k = \gamma_T/\gamma_R > 1$. It must be mentioned, though, that the value of γ_R used may be too large. It has not been subject to a direct measurement, and the values listed in Table 2.1.1 are based on the design values supplied by the manufacturer.

In order to investigate the mentioned discrepancies further, we performed a new series of calibrations of propellers "X" and "Y", with each calibration preceded by small changes in the propeller. Propeller "Ref" was used as a standard in all the tests.

The first test was to investigate the importance of the assumed two-axis symmetry of each propeller blade segment. Figure 2.1.3 shows the blade cross-section supplied by the manufacturer(a), and the modified cross-sections, (b) and (c). The second test was designed to study the influence of increased blade surface roughness. On propeller Y the sharp edges shown in Figure 2.1.3(a) were maintained while the surface marked 1 was roughened using coarse sand paper. Propeller X, featuring the blade cross-section shown on Figure 2.1.3(b), had all surfaces roughened in the same manner. In the third, and

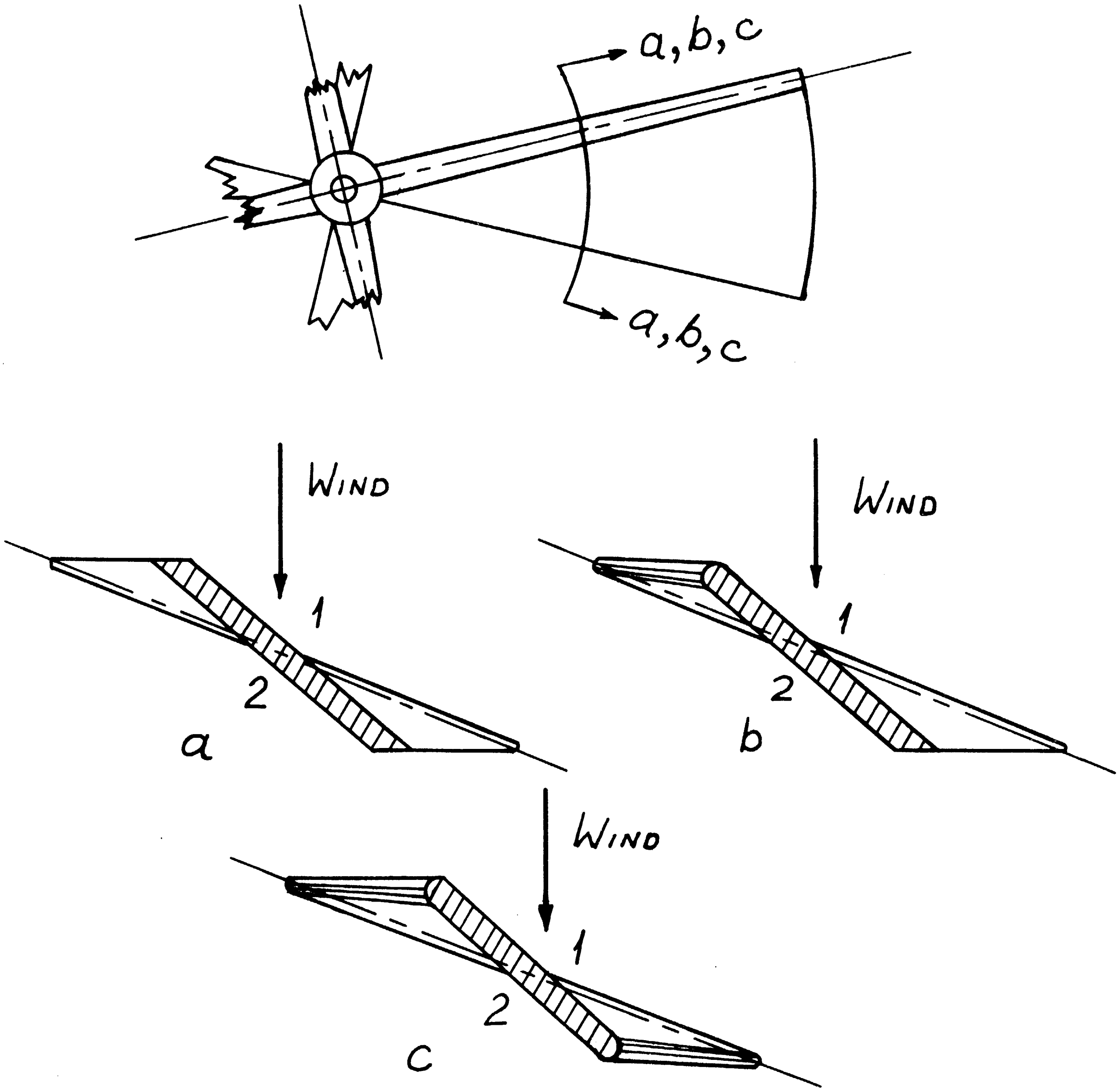

Figure 2.1.3
Propeller blade cross-sections.

last run, propeller X, still with rough surfaces, was given the blade cross-section shown as Figure 2.1.3(c).

Table 2.1.3 lists the obtained results. The original X propeller shows about 0.1 percent difference in sensitivity depending on the side of the propeller facing the wind. Pro-

Propeller	Calibration Specification				Results from Regression				
Polystyrene O.D. .228 m	Range			Ambient temp. $^\circ$C	γ_T	S.D. γ_T	ΔU m/s	S.D. ΔU m/s	$\frac{\gamma_T - \gamma_R}{\gamma_R} \times 100\%$
	min m/s	max m/s	No. of points						
X; surfaces 1 lead	1.48	11.26	7	27	.419	.001	.014	.003	-1.1
X; surfaces 1 lead; edges 1 round	.71	11.30	6	30	.419	.001	.006	.002	-1.1
X; surfaces 1 lead; edges 1 round; surfaces 1,2 rough	2.26	11.29	5	30	.424	.001	-.02	.01	.0
X; surfaces 1 lead; edges 1, 2 round; surfaces 1,2 rough	1.97	11.34	8	27	.427	.001	-.005	.008	.7
X; surfaces 2 lead	7.32	10.15	3	27	.419		.030		-1.2
X; surfaces 2 lead; edges 1 round	.71	11.30	6	30	.426	.001	.012	.004	.5
X; surfaces 2 lead; edges 1, 2 round; surfaces 1,2 rough	1.69	11.30	7		.426	.001	-.005	.002	.4
Y; surfaces 1 lead	1.48	11.26	7	27	.420	.001	.011	.005	- .9
Y; surfaces 1 lead; surfaces 1 rough	.71	11.30	6	30	.427	.001	-.010	.008	.7
Y: surfaces 2 lead	7.32	10.15	3	27	.423		.020		- .1
Y: surfaces 2 lead; surfaces 1 rough	.71	11.30	6	30	.424	.001	.003	.003	.0

Table 2.1.3

Calibration specification for altered polystyrene propellers peller Y indicates a 0.8% difference. (Analogous differences in sensitivity are obtained for other propellers, too.) By rounding the leading edges of the blades, the sensitivity does not change significantly, but when the rounded edge is trailing, we notice a decrease in speed of revolution of 1.7%. If, however, the blade surface roughness is increased, rounding of the trailing edge only results in a 0.7% decrease in speed.

Increased surface roughness alone will also decrease the indicated speed. With a rounded leading edge, roughening of all blade surfaces results in a 1.1% decrease of turning speed. Unmodified edges together with increases in surface roughness have a more pronounced influence on the speed, ranging from a 1.6% decrease, if the leading surfaces alone are roughened, to a 0.1% decrease with the trailing surface roughened.

These results do in our opinion indicate that the sharp-edged non-symmetrical blade cross-section generates separation of the flow across the trailing surface. Furthermore, the symmetry at the trailing edges for a zero incidence angle apparently results in a positive lift, and not a zero lift as assumed in Chapter 1. These statements imply that the propellers as delivered by the manufacturer do not respond sinusoidally if exposed to a sinusoidal wind field. By rounding the edges, the lift at a zero angle of incidence must decrease, since the speed of revolution drops more than one percent. This is equivalent to an increase in angle of incidence of the order of half a degree at the tip of the blades. The results listed in Table

2.1.3 do not specifically indicate that separation of the flow across the trailing surfaces is prevented by rounding the surface edges. Hence, we must emphasize the need for further investigations into the question of propeller response to accelerating and decelerating flow fields.

2.1.2 Distance Constants

Although the theory of Chapter 1.0 may be a too crude approximation to the actual behavior of the helicoid propellers, as already mentioned, it seems relevant at this stage to estimate the distance constants given by Equation (1.2.19).

Since we do not know the theoretical pitchfactor, γ_R, we shall prescribe the following values,

Propeller	γ_R	$k = \gamma_T/\gamma_R$
Aluminum	.47	1.02, 1.04, 1.06
Polystyrene	.42	1.02, 1.04, 1.06

Table 2.1.4
Pitchfactor for aluminum and polystyrene propellers

Furthermore, we assume a barometric pressure of 1013 mb and ambient temperature of 21°C yielding an air density of $\rho_a = 1.2$ kg/m^3.

In Table 2.1.5 we have listed the obtained results, while Figure 2.1.4 shows the distance constant for the two propeller types as functions of C_D/C_L^o and C_L^o. We notice that L for the aluminum propeller is about 3.6 times L for the polystyrene. Equation (1.2.19) indicates, however, that this number might be decreased by increasing γ_R or by diminishing ρ_m or b_1. If, for example, we double γ_R, which can be done by halving the propeller diameter, we obtain a 20% decrease of L. But by decreasing the propeller diameter, the blade thickness may also be diminished

Propeller	k	$I_1 + b_2/b_1 I_2$	C_D/C_L^o	W_o	$L \cdot C_L^o$
Aluminum	1.02	1.19	.017	.020	3.6 m
O.D. .114 m	1.04	1.19	.034	.038	3.4 m
	1.06	1.19	.054	.057	3.3 m
Polystyrene	1.02	.58	.020	.020	1.0 m
O.D. .100 m	1.04	.58	.038	.038	.9 m
	1.06	.58	.057	.057	.9 m

Table 2.1.5
Distance constants for aluminum and polystyrene propellers for value of k given in Table 2.1.4

without any loss in rigidity. Hence, a 0.10 m diameter aluminum propeller with a blade thickness of 0.0003 m should have a distance constant less than twice the one for the polystyrene propeller listed in Table 2.1.5.

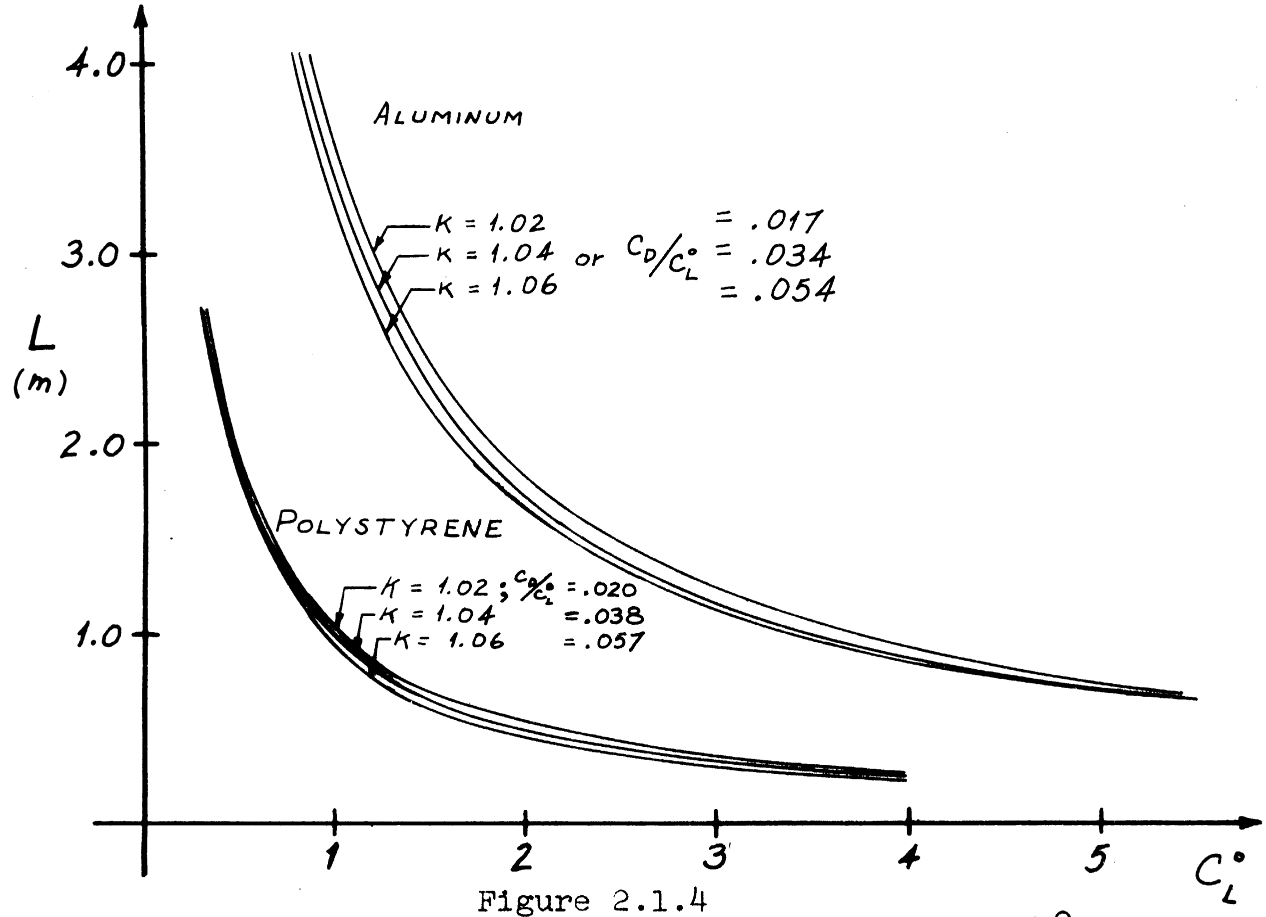

Figure 2.1.4
Distance constants as function of C_D and C_D/C_L^o.

2.1.3 Calibration for Non-Axial Flow

Having determined γ_T and ΔU for the propellers by calibration in axial flow, we are now going to consider non-axial flow. The performed measurements enable us, as already mentioned, to calculate $S(\theta)$ for angle increments of 5°, 10° or 15°. Table 2.1.6 lists the obtained results for angle increments of 5°. We notice the standard error (S.E.) to be relatively constant (0.001 - 0.003). The standard deviations (S.D.) for the polystyrene propellers seem larger than the S.D. for the aluminum propeller. This is probably due to the fact that only one aluminum propeller, compared to three polystyrene propellers, was investigated. Figures 2.1.5a and b show the obtained values of $S(\theta)$ versus the axial wind speed. We notice some scattering about the mean values, but apparently no trends at increasing velocity. The absolute scattering seems quite independent of the angle of attack. As a result, the relative accuracy of the measured mean values decreases from about a quarter of a percent for angles close to zero to about two percent for angles close to ninety degrees.

Angle θ degrees	Aluminum O.D. .200 m				Polystyrene O.D. .228 m			
	Measurements			Regression	Measurements			Regression
	$S(\theta)$	S.D.	S.E.	$S(\theta)$	$S(\theta)$	S.D.	S.E.	$S(\theta)$
0	1.000			1.000	1.000			1.000
5	.996	.001	<.001	.995	.993	.004	.002	.994
10	.981	.003	.001	.979	.975	.008	.003	.975
15				.953	.955	.008	.002	.948
20	.917	.003	.001	.917	.915	.005	.002	.914
25				.870	.872	.008	.003	.872
30	.810	.003	.001	.813	.817	.009	.002	.819
35				.746	.757	.004	.001	.753
40	.669	.003	.001	.674	.680	.005	.002	.678
45	.597	.004	.001	.601	.604	.010	.002	.599
50	.528	.004	.002	.531	.519	.007	.003	.521
55	.464	.007	.002	.467	.449	.009	.003	.449
60	.414	.004	.001	.408	.383	.006	.001	.381
65				.351	.322	.005	.002	.314
70	.286	.012	.004	.293	.245	.005	.002	.247
75	.226	.006	.002	.229	.181	.009	.002	.179
80	.162	.010	.004	.158	.116	.008	.002	.115
85	.086	.010	.003	.081	.049	.008	.003	.056
90	0.000			0.000	0.000			0.000

Table 2.1.6

Calibration results computed for aluminum and polystyrene propellers for non-axial flow.

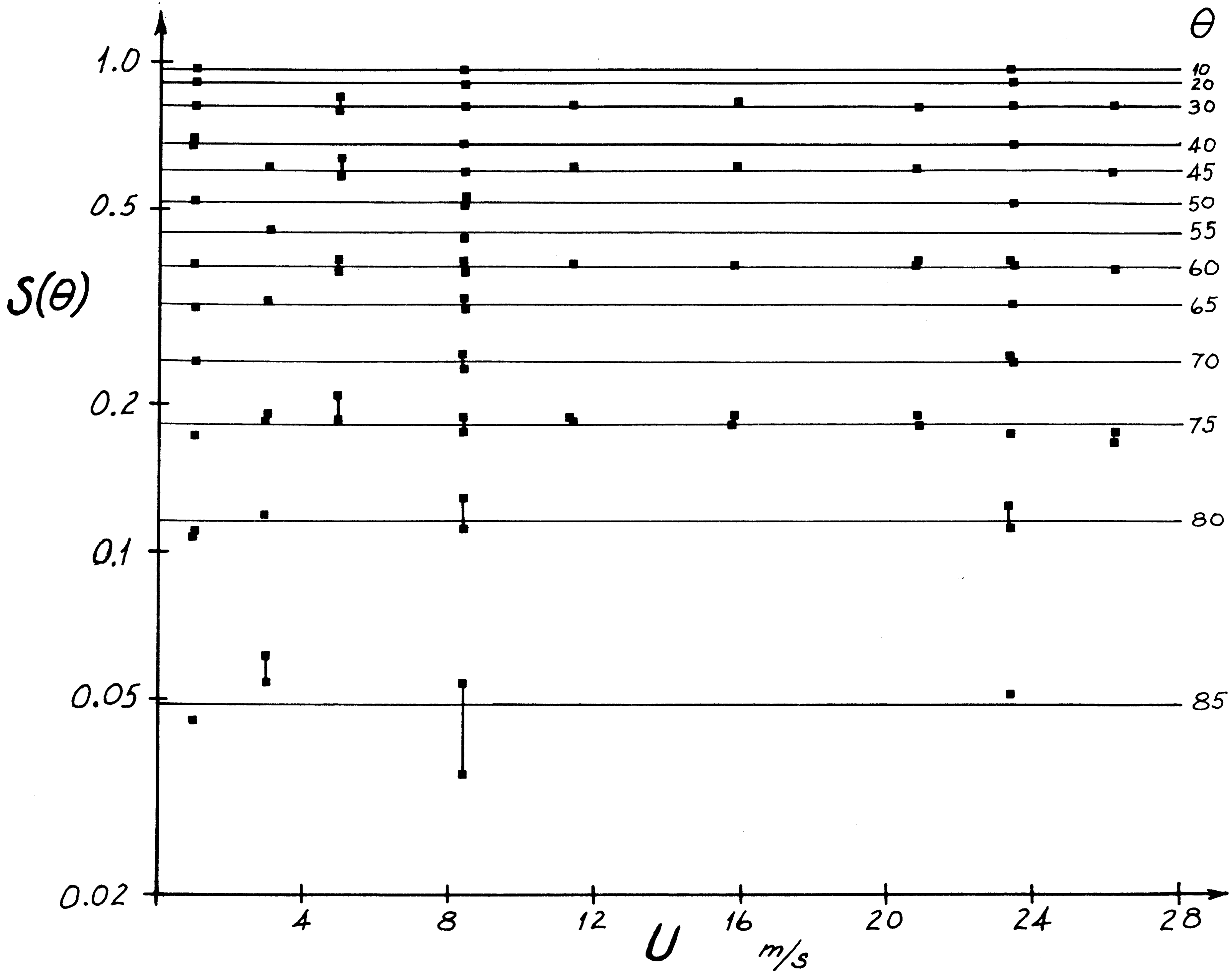

Figure 2.1.5a
Angular response versus wind speed for polystyrene propellers.

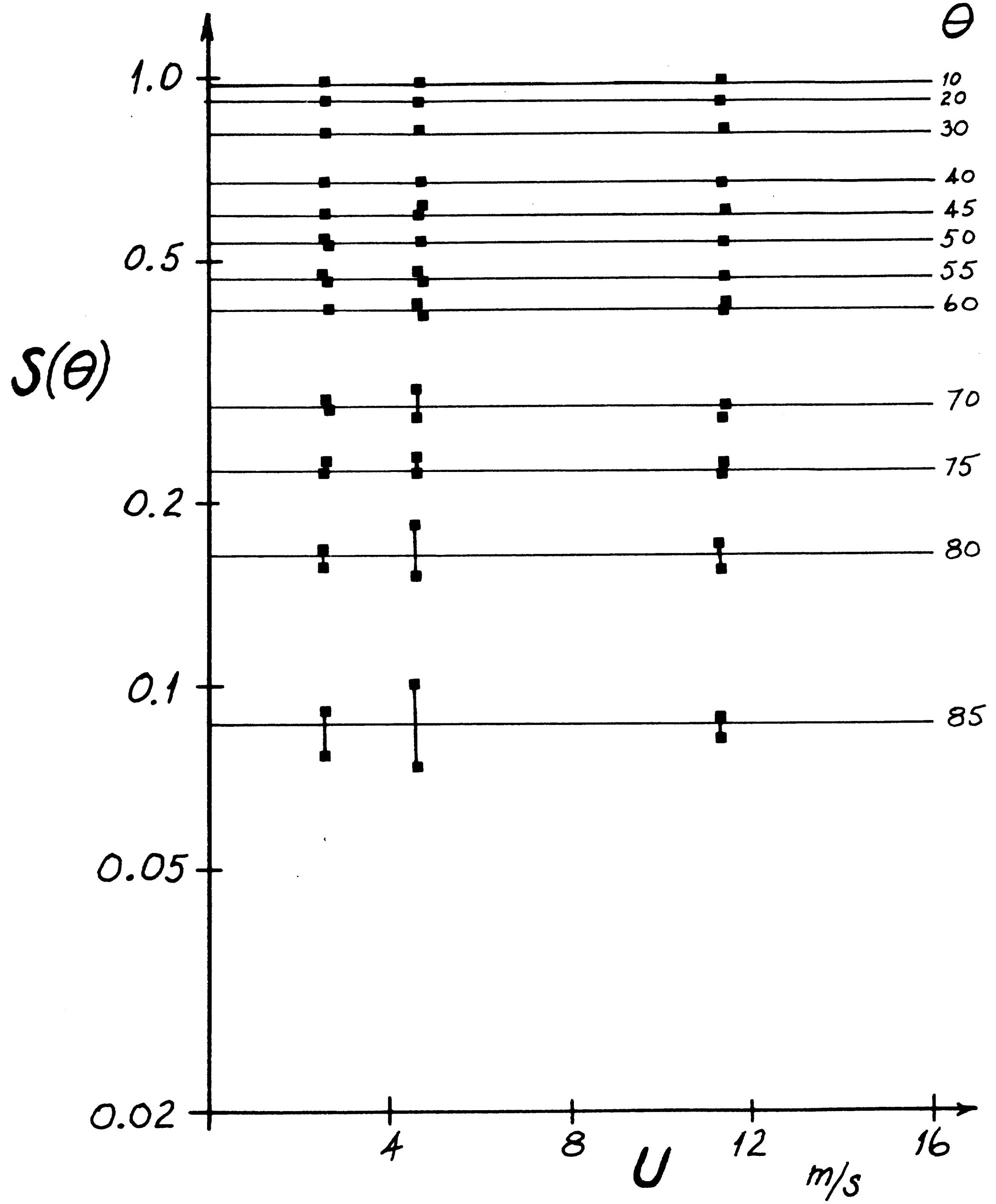

Figure 2.1.5b
Angular response versus wind speed for aluminum propellers.

2.1.4 The Angular Response Function

Based on the presented data, we may conclude that the helicoid propellers investigated have a calibration function for axial flow as predicted in Chapter 1. Concerning non-axial flow, the theoretical analysis, however, does not enable us to consider very large angles of attack. Hence we are totally dependent on the measurements when stating the following:

For all angles of attack ($|\theta| \leq 90^\circ$) the calibration function is given by

$$\gamma_T \cdot R \cdot \omega = S(\theta) \cdot (U - \Delta U), \tag{2.1.1}$$

where γ_T and ΔU depend exclusively upon the individual propellers and their measuring device, while $S(\theta)$ is unique for each propeller type, except for a small region about $\theta = 90^\circ$ (the stall region). Furthermore, the measurements indicate that

$$S(\theta) \leq \cos\theta$$

for all angles $|\theta| \leq 90^\circ$. In the following we shall outline a method by which we can obtain a mathematical expression for $S(\theta)$ based on measurements of $S(\theta)$. Principally,we approximate $S(\theta)$ by a finite Fourier series.

$$S(\theta) \simeq \sum_{n=0}^{n=m} a_n \cos n\theta + b_n \sin n\theta, \qquad (2.1.2)$$

where m is any positive integer chosen by us.

If we now assume $S(\theta)$ known (through measurements) for N equi-spaced angles between 0 and 90 degrees, we are able to determine sets of N Fourier constants, each composing a function which exactly satisfies the measured values of $S(\theta)$. By defining $S(\theta)$ for angles $|\theta| > 90^\circ$ we may, however, reduce the number of sets from infinity to one and at the same time achieve the most rapid converging set for a given angle increment.

We assume the angle increment $\Delta\theta$ given by

$$\Delta\theta = 90/N \text{ degrees}. \qquad (2.1.3)$$

For angles $|\theta| > 90^\circ$, $S(\theta)$ is defined by

$$S(\,(2qN \pm n)\Delta\theta) = -S(n\Delta\theta) \quad q = \pm 1, \pm 2, \ldots., \pm\infty$$

and

$$S(\,(4pN \pm n)\Delta\theta) = S(n\Delta\theta) \quad p = 0, \pm 1, \pm 2, \ldots., +\infty \qquad (2.1.4)$$

$$n = 0, 1, \ldots., N.$$

Equation (2.1.4) defines $S(\theta)$ for discrete given angles between $-\infty < \theta < \infty$ only. A finite Fourier series of N terms can, however, be determined to satisfy $S(\theta)$ at all these angles. Hence, by choosing a large enough N (i.e., avoiding aliasing about the harmonic value 2N), we can use a limited number of the harmonics in the finite Fourier series to describe $S(\theta)$ with an acceptable degree of accuracy for any angle $|\theta| \leq 90^{\circ}$.

By means of Equations (2.1.2) and (2.1.4) we obtain

$$S(m\Delta\theta) = \sum_{n=0}^{4N-1} a_n \cos nm\Delta\theta, \qquad (2.1.5)$$

since $S(m\Delta\theta)$ is symmetrical about $m = 0$.

By multiplying both sides of Equation (2.1.5) by $\cos(mj\Delta\theta)$ and summing over m, we obtain

$$\sum_{m=0}^{4N-1} S(m\Delta\theta)\cos(mj\Delta\theta) =$$

$$\tfrac{1}{2}\sum_{n=0}^{4N-1} a_n \sum_{m=0}^{4N-1} \left\{\cos m\,\frac{n+j}{2}\Delta\theta + \cos M\,\frac{n-j}{2}\Delta\theta\right\} = \qquad (2.1.6)$$

$$\begin{cases} 4Na_o; & j = 0 \\ 2Na_n; & j = n. \end{cases}$$

Thus,

$$a_o = \frac{1}{4N} \sum_{m=0}^{4N-1} S(m\Delta\theta)$$

and (2.1.7)

$$a_n = \frac{1}{2N} \sum_{m=0}^{4N-1} S(m\Delta\theta) \cos(nm\Delta\theta) \cdot$$

Substituting Equation (2.1.4) into Equation (2.1.7) yields ($n \neq 0$).

$$a_n = \frac{1}{2N} \sum_{m=0}^{N-1} S'(m\Delta\theta) \Big\{\cos(nm\Delta\theta) - \cos((2N-n)m\Delta\theta) - \cos((2N+n)m\Delta\theta) + \cos((4N-n)n\Delta\theta)\Big\}, \tag{2.1.8}$$

where $S'(m\Delta\theta) = \begin{cases} \frac{1}{2}S(0) \\ S(m\Delta\theta) \text{ for } m = 0. \end{cases}$

Following some simple algebra we finally obtain

$$a_n = \frac{2}{N} (-1)^{\frac{n-1}{2}} \sum_{m=0}^{N-1} S'(m\Delta\theta) \sin(n(N-m)\Delta\theta) \tag{2.1.9}$$

for $n = 1, 3, 5, \ldots, 2N-1$;

and $a_n = 0$

for $n = 0, 2, 4, \ldots, 2N$.

Having derived Equation (2.1.9), we approximate $S(\theta)$ by

$$S(\theta) = \sum_{m=1}^{N_1} a_{2m-1} \cos(2m-1)\theta, \tag{2.1.10}$$

where $N_1 \leq N$ is chosen according to the numerical values of a_{2m-1} for $N_1 < m \leq N$; enabling us to reproduce $S(\theta)$ at all angles with an acceptable accuracy. If $N_1 = N$, Equation (2.1.10) merely acts as an interpolation formula relating all non-measured $S(\theta)$ values to the measured ones.

If we assume the statistical distribution of $S(n\Delta\theta)$ measured to be normal, we may choose N_1 as the smallest value for which Equation (2.1.10) approximates most of the measured mean values within 95 percent confidence intervals.

Let us assume the mean values for $S(n\Delta\theta)$ distributed with a variance $\sigma^2_{\overline{S(n\Delta\theta)}}$, which is constant for $0 < n\Delta\theta < 90$, and null for $n\Delta\theta = 0$ and $n\Delta\theta = 90$. Then Equation (2.1.9) enables us to calculate the probability distribution of a_n. We obtain $\overline{a_n} = a_n$ as given by Equation (2.1.9), while

$$\sigma^2_{\overline{a_n}} = \left(\frac{2}{N}\right)^2 \cdot \sigma^2_{\overline{S(n\Delta\theta)}} \sum_{m=1}^{N-1} \sin^2(n(N-m)\Delta\theta),$$

or since the summation is independent of $n\Delta\theta$,

$$\sigma^2_{\overline{a_n}} = \sigma^2_{\overline{S(n\Delta\theta)}} \cdot 2 \cdot (N-1)/N^2. \tag{2.1.11}$$

By means of Equation (2.1.10) we may now express the mean value of any $S(\theta)$ by the mean value of a_n as a function of N_1, and analogously the variance of the mean values by the variance of $\overline{a}_{2m-1}$. We get

$$\overline{S(\theta,N_1)} = \sum_{m=1}^{N_1} a_{2m-1} \cos (2m-1)\theta$$

and (2.1.12)

$$\sigma^2_{\overline{S(\theta,N_1)}} = \sigma^2_{\overline{a}_n} \sum_{m=1}^{N_1} \cos^2 (2m-1)\theta .$$

Finally, the 95% confidence intervals as functions of θ and N_1 are given by

$$\text{C.I.}_{.95} \left\{ \overline{S(\theta,N_1)} - 1.96\, \sigma_{\overline{S(\theta,N_1)}} ; \ \overline{S(\theta,N_1)} + 1.96\, \sigma_{\overline{S(\theta,N_1)}} \right\} . \qquad (2.1.13)$$

In the following, this outlined procedure is performed on the measurements of the polystyrene propellers. In Table 2.1.6 the mean values of $S(n\Delta\theta)$ are listed, and, as mentioned already, the S.E. seems pretty well independent of $(n\Delta\theta)$. We may thus approximate

$$\sigma^2_{\overline{S(n\Delta\theta)}} \simeq 4 \times 10^{-6} .$$

Equation (2.1.11) hence yields

N = 6	N = 9	N = 18
$\sigma_{\bar{a}_n}$	$\sigma_{\bar{a}_n}$	$\sigma_{\bar{a}_n}$
0.0011	0.0009	0.0006

Table 2.1.7
Computations of $\sigma_{\bar{a}_n}$ with Equation 2.1.11.

By means of Equations (2.1.12) and (2.1.13), the confidence intervals for θ equi-spaced between 0 and 90°, with angle increments of 5°, are calculated for $N = N_1 = 6$; $N = 9$, $N_1 = 5, 6, 9$ and $N = 18$, $N_1 = 5, 6, 13$. The results are listed in Table 2.1.8. The underlined numbers mean that the measured $S(\theta)$ fall outside the particular confidence limits.

For $N = 6$, where the highest detectable harmonic has less than three full periods for $0 \leq \theta \leq 90^\circ$, we notice acceptance at very few angles in addition to the ones used in calculating the Fourier coefficients. On the other hand, if we increase the number of wave numbers by 50% ($N = 9$), a change from $N_1 = 5$ to $N_1 = 6$ causes a very pronounced improvement in the approximation; while a change from $N_1 = 6$ to $N_1 = 9$ causes only small refinements. It is evident that except for $\theta = 85^\circ$ there is a trend of improved approximation with increasing N_1 for all non-accepted angles. This implies that the discrepancies between the calculated $S(\theta)$ and the measured one can only be removed by wave-numbers still

θ	S(θ)	N = 6		N = 9						N = 18					
		N_1 = 6		N_1 = 5		N_1 = 6		N_1 = 9		N_1 = 5		N_1 = 6		N_1 = 13	
Degrees	Measured	C.I.$_{.95}$		C.I.$_{.95}$		C.I.$_{.95}$		C.I.$_{.95}$		C.I.$_{.95}$		C.I.$_{.95}$		C.I.$_{.95}$	
0	1.000	.995	1.005	.992	1.000	.996	1.004	.995	1.005	**.993**	**.998**	.998	1.004	.996	1.004
5	.993	.991	.999	.988	.995	.990	.997	.990	.997	.989	.994	.992	.997	.990	.995
10	.975	**.977**	**.983**	.974	.980	.973	.978	.972	.979	**.976**	**.980**	.974	.978	.973	.979
15	.955	.951	.959	.950	.955	**.945**	**.951**	**.946**	**.953**	.953	.956	**.947**	**.952**	.950	.956
20	.915	**.916**	**.924**	.915	.921	.911	.917	.911	.919	**.918**	**.922**	.914	.918	.914	.920
25	.872	.870	.877	.869	.874	.869	.875	.867	.875	.871	.875	.872	.876	.867	.873
30	.817	.813	.821	.812	.817	.816	.822	.813	.821	.814	.818	**.819**	**.823**	.815	.822
35	.757	**.748**	**.755**	**.747**	**.752**	.750	.757	.750	.758	**.748**	**.752**	.753	.757	.753	.759
40	.680	.676	.683	.674	.680	.675	.681	.677	.684	.676	.680	.677	.681	.678	.684
45	.604	.600	.608	.599	.605	**.596**	**.602**	**.595**	**.603**	.602	.605	**.598**	**.602**	.600	.606
50	.519	**.524**	**.532**	**.523**	**.528**	.518	.525	.515	.523	**.526**	**.530**	**.521**	**.525**	.518	.524
55	.449	**.451**	**.458**	.448	.454	.446	.452	.444	.452	**.452**	**.455**	.449	.453	.443	.449
60	.383	.379	.387	**.376**	**.382**	.378	.384	.379	.387	.379	.383	.382	.386	.383	.389
65	.322	**.310**	**.318**	**.307**	**.312**	**.311**	**.317**	**.312**	**.320**	**.310**	**.314**	**.315**	**.319**	.317	.323
70	.245	.243	.250	.241	.246	.244	.250	.242	.249	.243	.247	**.246**	**.250**	.243	.249
75	.181	.177	.185	.178	.184	.176	.183	.173	.181	.179	.183	.177	.181	.178	.184
80	.116	.114	.123	.116	.122	.112	.118	.112	.120	**.117**	**.121**	.112	.116	.113	.119
85	.049	**.056**	**.061**	**.058**	**.061**	**.053**	**.058**	**.055**	**.062**	**.058**	**.060**	**.053**	**.056**	.046	.053
90	.000	.000	.000	.000	.000	.000	.000	.000	.000	.000	.000	.000	.000	.000	.000

Table 2.1.8

Computations of confidence intervals for θ and 0 and 90 degrees.

higher than 17. Thus, for N = 18 we notice acceptance at all measured angles for $N_1 \geq 13$, indicating that wave numbers as high as 25 are needed to describe $S(\theta)$. Again, changing N_1 from 5 to 6 improves the approximation significantly.

Since the noticed discrepancies at $N_1 = 6$ are small for N = 9 (and even smaller for N = 18), probably very little overall accuracy is lost by only using 6 parameters in the approximation of $S(\theta)$. We hence recommend the following approximation of $S(\theta)$.

$$S(\theta) = \sum_{m=1}^{6} a_{2m-1} \cos (2m-1)\theta, \tag{2.1.14}$$

where two sets of values of a_{2m-1} are listed in Table 2.1.9.

Aluminum				Polystyrene							
N = 9				N = 9				N = 18			
a_1	.9375	b_0	.9304	a_1	.9285	b_0	.6286	a_1	.9302	b_0	.6170
a_3	.0596	b_2	-.7960	a_3	.0798	b_2	1.2638	a_3	.0790	b_2	1.5096
a_5	.0142	b_4	1.2432	a_5	-.0077	b_4	-5.3595	a_5	-.0078	b_4	-6.5160
a_7	-.0139	b_6	1.0048	a_7	-.0046	b_6	12.6617	a_7	-.0044	b_6	14.9210
a_9	.0016	b_8	-2.4064	a_9	-.0004	b_8	-12.8128	a_9	-.0013	b_8	-14.7840
a_{11}	.0010	b_{10}	1.0240	a_{11}	.0045	b_{10}	4.6182	a_{11}	.0051	b_{10}	5.2531

Table 2.1.9
Sets of values of a_{2m-1} and b_{2m-2} for aluminum and polystyrene propellers.

These two functions obtained from the sets of values given in the table do not deviate much, but probably the one obtained for $N = 18$ will give a slightly increased accuracy, especially for small angles.

For computational reasons, it is advantageous to express Equation (2.1.14) as a polynomial series in $\cos\theta$.

$$S(\theta) = \cos\theta \cdot \sum_{m=1}^{6} b_{2m-2} \cos^{2m-2}(\theta) \qquad (2.1.15)$$

By some simple but laborious reductions, we obtain the following relations between a_{2m-1} and b_{2m-2}

$$\begin{aligned} b_0 &= a_1 - 3a_3 + 5a_5 - 7a_7 + 9a_9 - 11a_{11} \\ b_2 &= 4\,\{a_3 - 5a_5 + 14a_7 - 30a_9 + 55a_{11}\} \\ b_4 &= 16\,\{a_5 - 7a_7 + 27a_9 - 77a_{11}\} \\ b_6 &= 64\,\{a_7 - 9a_9 + 44a_{11}\} \\ b_8 &= 256\,\{a_9 - 11a_{11}\} \\ b_{10} &= 1024\,a_{11} \end{aligned} \qquad (2.1.16)$$

In Table 2.1.9 columns of b_{2m-2} are also listed.

For the sake of completeness, $S(\theta)$ for the aluminum propeller has also been calculated. Also, Figure (2.1.6) shows the angular response functions as they look when calculated by means of Equation (2.1.15) for $N = 9$. The ordinates in these calculations are listed in Table 2.1.6 for immediate comparison to the measured values. We notice that the actual response for the aluminum propellers does not deviate very much from the response of the poly-

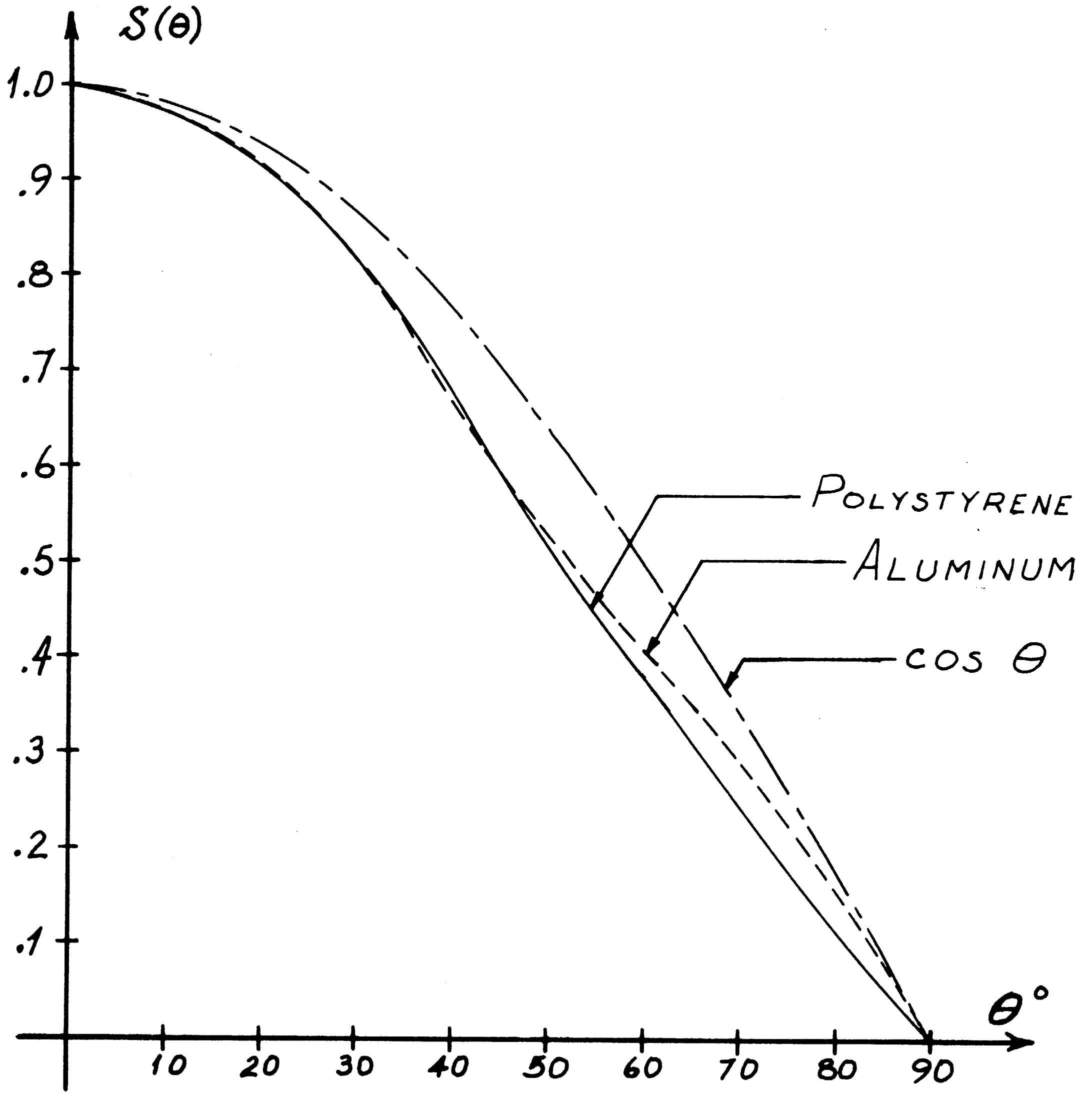

Figure 2.1.6
Angular response functions.

styrene propeller for angles less than 50°. For larger angles, however, the aluminum propeller has an increasingly higher response, although still less than cosine response. For θ close to 90° the aluminum propeller response is very closely given by $S(\theta) = 0.93 \cos\theta$ while the polystyrene propellers follow $S(\theta) = 0.62 \cos\theta$. In this region, therefore, the aluminum propellers apparently have a 50% higher response than the polystyrene propellers.

3.0 A Three-Dimensional Velocity Sensor

In this chapter we shall make use of the results concerning the helicoid propeller's response to non-axial flow.

We may write the governing equation as follows

$$S(\theta) \cdot \sqrt{\overline{U} \cdot \overline{U}} = \omega R \gamma_T + \Delta U \, S(\theta), \qquad (3.0.1)$$

where $\theta = \cos^{-1} \left\{ p \frac{U}{|\overline{U}|} + q \frac{V}{|\overline{U}|} + r \frac{W}{|\overline{U}|} \right\}$,

and (p,q,r) are the direction cosines of the propeller axis. Equation (3.0.1) indicates that if we at all times had three independent propellers measuring the same velocity vector, we could solve the three equations with respect to $\overline{U} = (U, V, W)$. Usually, one of the problems in three-dimensional velocity sensing is the alignment of the probe. In the above-mentioned procedure, this problem is of course not eliminated, but its effects on the quality of the measurements are diminished because we are at all times measuring the complete velocity vector and relating it to the very accurately known geometry of the three-propeller sensor. Thus, without making any assumptions on the spatial alignment of the sensor, we are able to calculate the complete Reynolds' tensor as it is observed by the sensor. Later on, if we decide to compare elements of this tensor with other measurements, we can then make our alignment assumptions and rotate the coordinate system of observation accordingly.

It must be emphasized, however, that the Reynolds' tensor measured in this way is complete only to the degree of spatial resolution determined by the three-propeller sensor.

3.1 A Theory of Three-Dimensional Velocity Sensing by Means of a Three-Propeller Sensor

Let us assume three propellers are mounted spatially with their axes merging to the origin of a right-angled coordinate system, from here on called the reference system. Figure 3.1.1 visualizes the set up.

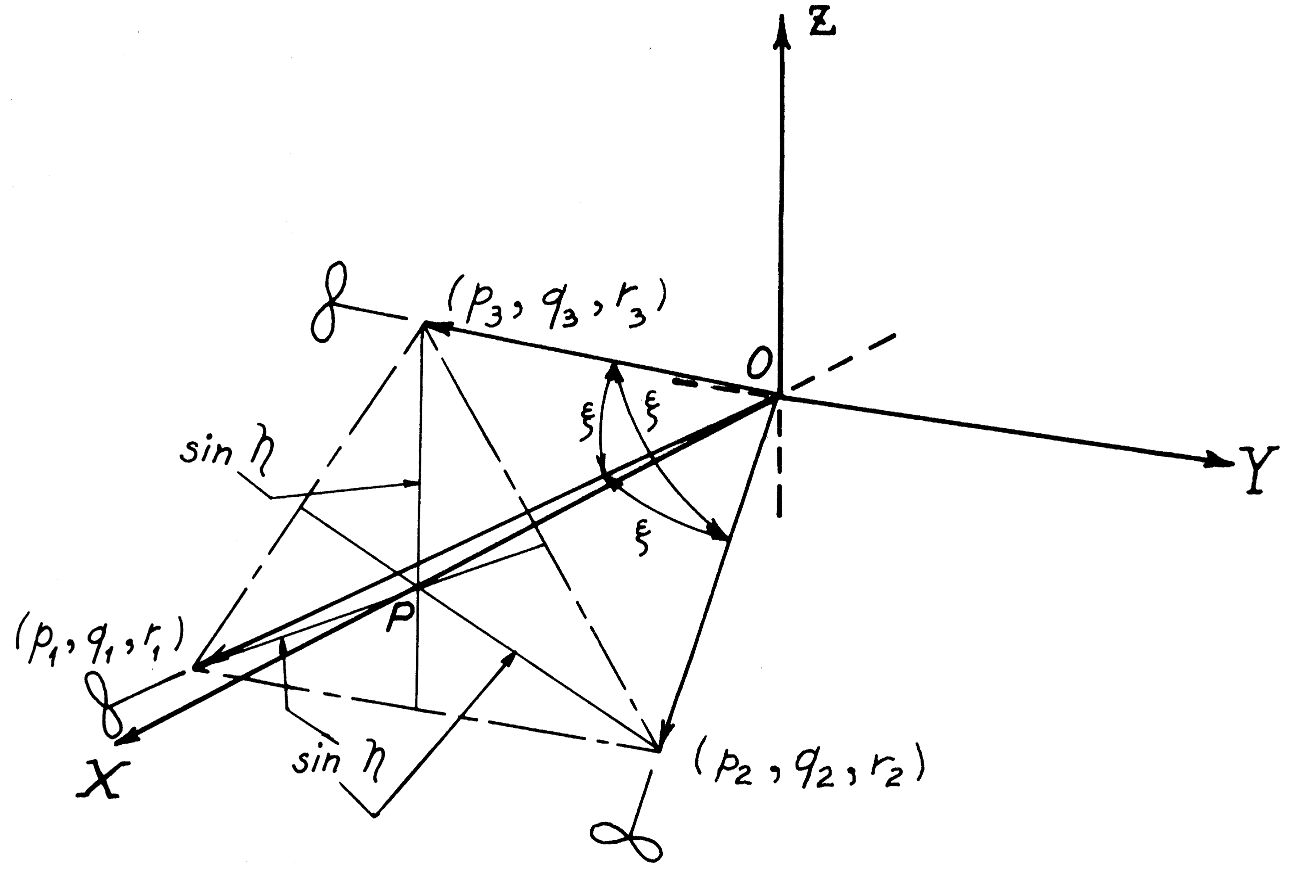

Figure 3.1.1
Reference coordinate system for the three-propeller sensor.

(p_1, q_1, r_1), (p_2, q_2, r_2) and (p_3, q_3, r_3) are the direction cosines of the three propeller axes. These axes constitute a not necessarily right-angled coordinate system. Without loss of generality, we may orient the axes in such a way that the following relations prevail.

$$\begin{aligned} p_1p_2 + q_1q_2 + r_1r_2 &= \cos \xi \\ p_1p_3 + q_1q_3 + r_1r_3 &= \cos \xi \\ p_2p_3 + q_2q_3 + r_2r_3 &= \cos \xi \end{aligned} \tag{3.1.1}$$

$$\begin{aligned} p_1 &= \cos \eta \\ p_2 &= \cos \eta \\ p_3 &= \cos \eta \end{aligned} \tag{3.1.2}$$

$$\begin{aligned} q_3 &= 0 \\ q_2 + q_1 &= 0 \\ r_1 - r_2 &= 0 \end{aligned} \tag{3.1.3}$$

Equations (3.1.1) express that the angle between any adjacent axes is ξ. Equations (3.1.2) denote that all axes have the same numerical slope toward the X-axis. Finally, Equations (3.1.3) express the symmetry and absence of symmetry in the chosen position of the probe system. Since direction cosines by definition are unit vectors, we are able to express all coordinates by ξ or η. We get:

$$\begin{aligned} (p_1, q_1, r_1) &= (\cos\eta;\ -\sqrt{3}/2\,\sin\eta;\ -\tfrac{1}{2}\sin\eta) \\ (p_2, q_2, r_2) &= (\cos\eta;\ \sqrt{3}/2\,\sin\eta;\ -\tfrac{1}{2}\sin\eta) \\ (p_3, q_3, r_3) &= (\cos\eta;\ 0\ ;\ \sin\eta), \end{aligned} \tag{3.1.4}$$

in which we already have incorporated

$$\cos^2\eta - \tfrac{1}{2}\sin^2\eta = \cos\xi. \tag{3.1.5}$$

The instantaneous wind vector is assumed to have direction cosines as follows:

$$\frac{-\bar{U}}{|\bar{U}|} = (\alpha, \beta, \gamma), \tag{3.1.6}$$

where $-\bar{U}$ denotes a wind direction toward the origin. Certain limitations are to be imposed upon $\bar{U}$ since we do not consider "reverse" flow, meaning a flow that forces any of the propellers to stop or reverse its direction of turning (positive directions of turning are obtained by a flow directed toward the origin parallel to the X-axis). If we assume all propellers to have the same threshold region of angles of attack, i.e., $\theta_o \leq \theta_i \leq 90^\circ$, where index i denotes the propeller number ($i = 1, 2, 3$), we can define the portion of space within which any wind will force the propellers to turn in a positive direction by the following inequalities:

$$\tan |Az| \leq \sqrt{3} \left\{ \cot\eta - \frac{\cos\theta_o}{\sin\eta \cos El} \right\} \tag{3.1.7}$$

$$- \left\{ \cot\eta \cos Az - \frac{\cos\theta_o}{\sin\eta \cos El} \right\} \leq \tan El \leq 2 \left\{ \cot\eta \cos Az - \frac{\cos\theta_o}{\sin\eta \cos El} \right\},$$

where

$$(\alpha, \beta, \gamma) = (\cos El \cos Az, \cos El \sin Az, \sin El), \tag{3.1.8}$$

i.e., the direction cosines expressed by an azimuth and an elevation angle in the reference coordinate system. Figure 3.1.2 shows acceptable Az and El angles for θ_o assumed equal to 90° and 88°, and $\eta = 15^\circ$. On Figure 3.1.2, the solid curve separates the acceptable region from the non-acceptable region for $\theta_o = 90^\circ$, i.e., at least one propeller is standing still. The dashed curve accordingly separates the two regions for $\theta_o = 88^\circ$. This means that a three-propeller sensor, with an aspect angle of 30°, may be used in measurements of a fluctuating flow field if any instantaneous wind direction does not exceed the acceptable region

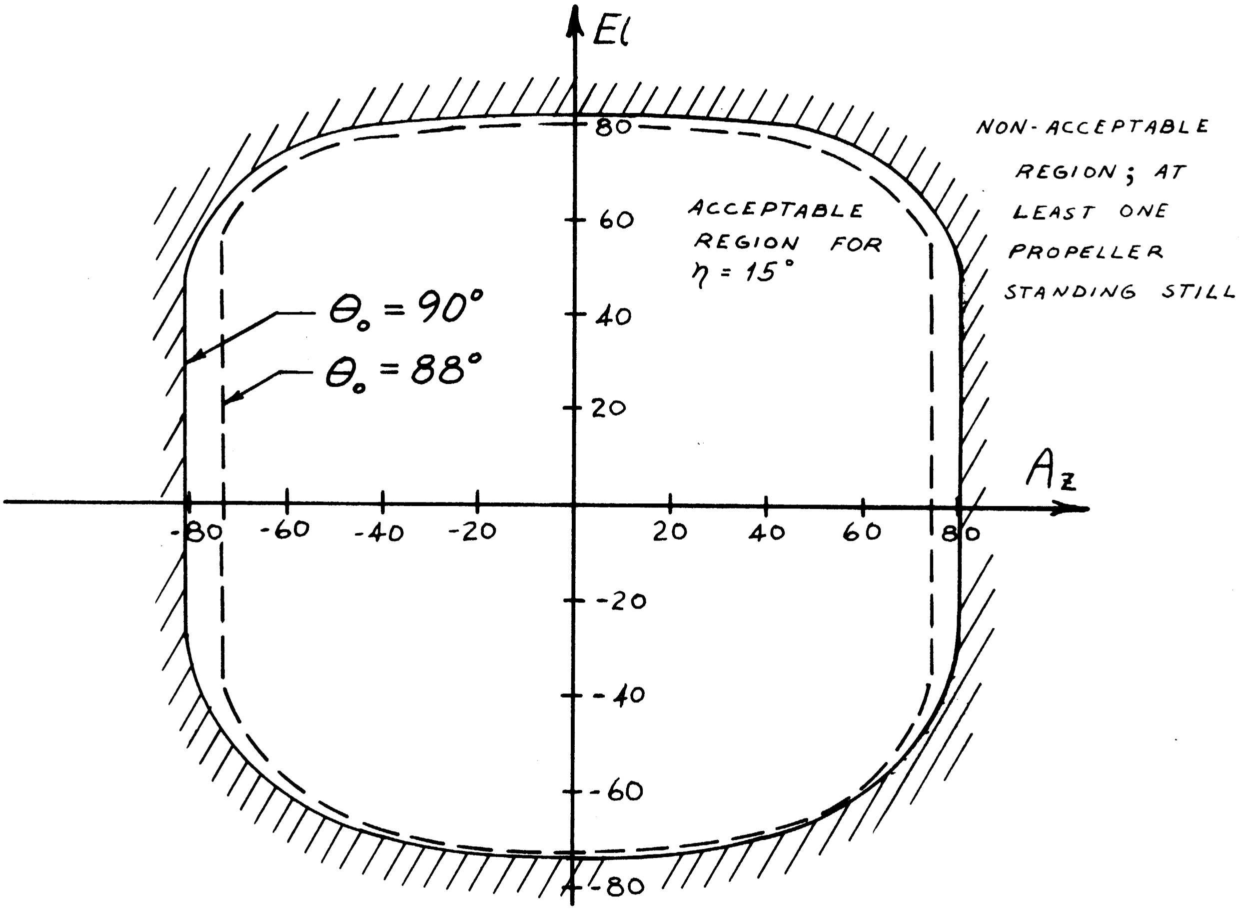

Figure 3.1.2
Angular working space of the 30° UVW.

of elevation and azimuth angles. Introducing the angles of attack of the wind vector (Equation (3.1.6)) toward the three propeller axes (Equation (3.1.4)) as ($\cos\theta_1$, $\cos\theta_2$, $\cos\theta_3$), we are able to express (a, β, γ) by these angles. We obtain

$$\alpha = \frac{\cos\theta_1 + \cos\theta_2 + \cos\theta_3}{3\cos\eta}$$

$$\beta = \frac{\cos\theta_2 - \cos\theta_1}{\sqrt{3}\sin\eta} \qquad (3.1.9)$$

$$\gamma = \frac{2\cos\theta_3 - (\cos\theta_1 + \cos\theta_2)}{3\sin\eta} \, .$$

Finally, the general calibration equation (Equation (3.0.1)) combined with Equation (3.1.9) enables us to write down the following iteration scheme by which a digital computer within a reasonable time can calculate the wind vector.

The following substitutions are just meant to clarify the equations

$$(\Omega_1, \Omega_2, \Omega_3) = |\bar{U}| \cdot (S(\theta_1), S(\theta_2), S(\theta_3)), \tag{3.1.10a}$$

or

$$\begin{pmatrix} \Omega_1 \\ \Omega_2 \\ \Omega_3 \end{pmatrix} = \begin{pmatrix} \omega_1 R\gamma_{T1} + \Delta U_1 \ S(\theta_1) \\ \omega_2 R\gamma_{T2} + \Delta U_2 \ S(\theta_2) \\ \omega_3 R\gamma_{T3} + \Delta U_3 \ S(\theta_3) \end{pmatrix} . \tag{3.1.10b}$$

From Equation (2.1.15) we may define

$$K\,(\cos\theta_i, \cos\theta_j) = \frac{\sum_{m=1}^{6} b_{2m-2} \cos^{2m-2}\theta_i}{\sum_{m=1}^{6} b_{2m-2} \cos^{2m-2}\theta_j}, \tag{3.1.11}$$

which leads to

$$S(\theta_i)\cdot\cos\theta_j = S(\theta\ )\cdot\cos\theta_i \cdot K(\cos\theta_i, \cos\theta_j). \qquad (3.1.12)$$

Hence Equations (3.1.10a) and (3.1.12) yield

$$\Omega_i \cos\,\theta_j = \Omega_j \cos\,\theta_i \cdot K\,(\cos\,\theta_i, \cos\,\theta_j). \qquad (3.1.13)$$

Knowing that Equation (3.1.9) defines a unit vector, we obtain after some simple rearrangements

$$\left(\sum_{i=1}^{3} \cos\theta_i\right)^2 + 3\cos^2\eta \left\{\sum_{i\neq j}^{3} \tfrac{1}{2}(\cos\theta_i - \cos\theta_j)^2 - \sum_{i=1}^{3} \cos^2\theta_i\right\} \qquad (3.1.14)$$

$$= 9/4\ \sin^2 2\eta.$$

Assuming the instantaneous wind vector is within the space defined on Figure 3.1.2, at least one propeller will be turning, i.e., the angle of attack is smaller than θ_0. If we therefore denote the turning propeller as No. A, we obtain the following equation of iteration for estimation of $\cos\theta_A$

$$\cos\theta_A = \frac{3\sin 2\eta}{2\sqrt{D + 3\cos^2\eta\,(E - F)}}\,, \qquad (3.1.15)$$

$$D = \left\{ \sum_{i=1}^{3} \frac{\Omega_i}{\Omega_A}\, K\,(\cos\theta_A, \cos\theta_i) \right\}^2 ,$$

$$E = \sum_{i \neq j}^{3} \tfrac{1}{2} \left(\frac{\Omega_i}{\Omega_A}\, K\,(\cos\theta_A, \cos\theta_i) - \frac{\Omega_i}{\Omega_A}\, K\,(\cos\theta_A, \cos\theta_i) \right)^2 ,$$

$$F = \sum_{i=1}^{3} \left(\frac{\Omega_i}{\Omega_A} \right)^2 K^2\,(\cos\theta_A, \cos\theta_i).$$

The advantage of this formulation is that all three angles: θ_1, θ_2 and θ_3 appear only implicitly through cosine functions raised to different powers. That means a reduction in computer time per iteration step, since multiplication of numbers demand only a small fraction of the time consumed by evaluating the sine or the cosine for specific angles.

A complete iteration step is as follows:

a) The former estimates of $\cos\theta_1$, $\cos\theta_2$ and $\cos\theta_3$ supply us with new estimates of $S(\theta_1)$, $S(\theta_2)$ and $S(\theta_3)$ through Equation (2.1.15). (Initially $(\cos\theta_1, \cos\theta_2, \cos\theta_3) = (1, 1, 1)$).

b) Equations (3.1.10b) supply us with new estimates of Ω_1, Ω_2 and Ω_3, which together with Equation (3.1.11) enable us to compute

c) $\frac{\Omega_i}{\Omega_A} K(\cos\theta_A, \cos\theta_i)$ from Equation (3.1.13).

d) Equation (3.1.15) then completes the iteration step by yielding a better value of $\cos\theta_A$.

e) Through Equation (3.1.13) we finally obtain new estimates of $\cos\theta_i$, and one more iteration step may begin.

The described iteration scheme converges, in most cases, fairly rapidly. For $\eta = 15^{\circ}$ an accuracy of 99.99% is achieved through no more than 25 iteration steps. In most cases an accuracy of 99.90% is probably sufficient, which of course will cut down the number of iterations (20 steps compared to 25).

Having found $\cos\theta_i$ with sufficient accuracy, Equations (3.1.9) and (3.1.6) then give us the components of $\overline{U}$ in the reference coordinate system, and, as mentioned earlier, statistical evaluations on these components are self-sustaining. In most cases, however, we want to work in a coordinate system determined by the mean wind and a horizontal plane. This requirement, of course, introduces an alignment problem. By using a simple rotation of the reference system about an appropriate axis, however, we can always achieve self-sustained vector components. If these components individually do not display assumed properties, the reason might be that the true alignment of the reference system to any chosen system is not known.

3.2 Experimental Investigation of Three-Dimensional Velocity Measurements by Means of a Three-Propeller Sensor

Prior to measurements in a turbulent flow using a three-propeller sensor, we considered it important to test the validity of the sensor's calibration by measuring the effects of a constant velocity on the sensor for different angles of attack.

With this purpose in mind we considered two systems. One is the commerically available three-propeller system designed by G. C. Gill and manufactured by R. M. Young Company, Traverse City, Michigan (3). It is shown in Figure 3.2.1. This system we shall designate as the Orthogonal UVW sensor. We have discussed earlier some of the disadvantages of the Orthogonal UVW sensor when used in a normal mode of operation (Chapter 2). With the desire to eliminate some of these disadvantages without decreasing the performance characteristics of the propeller sensors, we decided to modify the design of the UVW sensor with the following requirements:

(a) The modified UVW should only be operated in non-reversible flow fields, i.e., all three propellers should always rotate in a positive direction.

(b) Since the dynamic response of the helicoid propeller sensor is best in axial flow (see Chapter 1.2), and since the percentage error in the angular response function is smallest for close to axial flow, any acceptable flow direction should always attack at least one propeller in a close-to-axial direction.

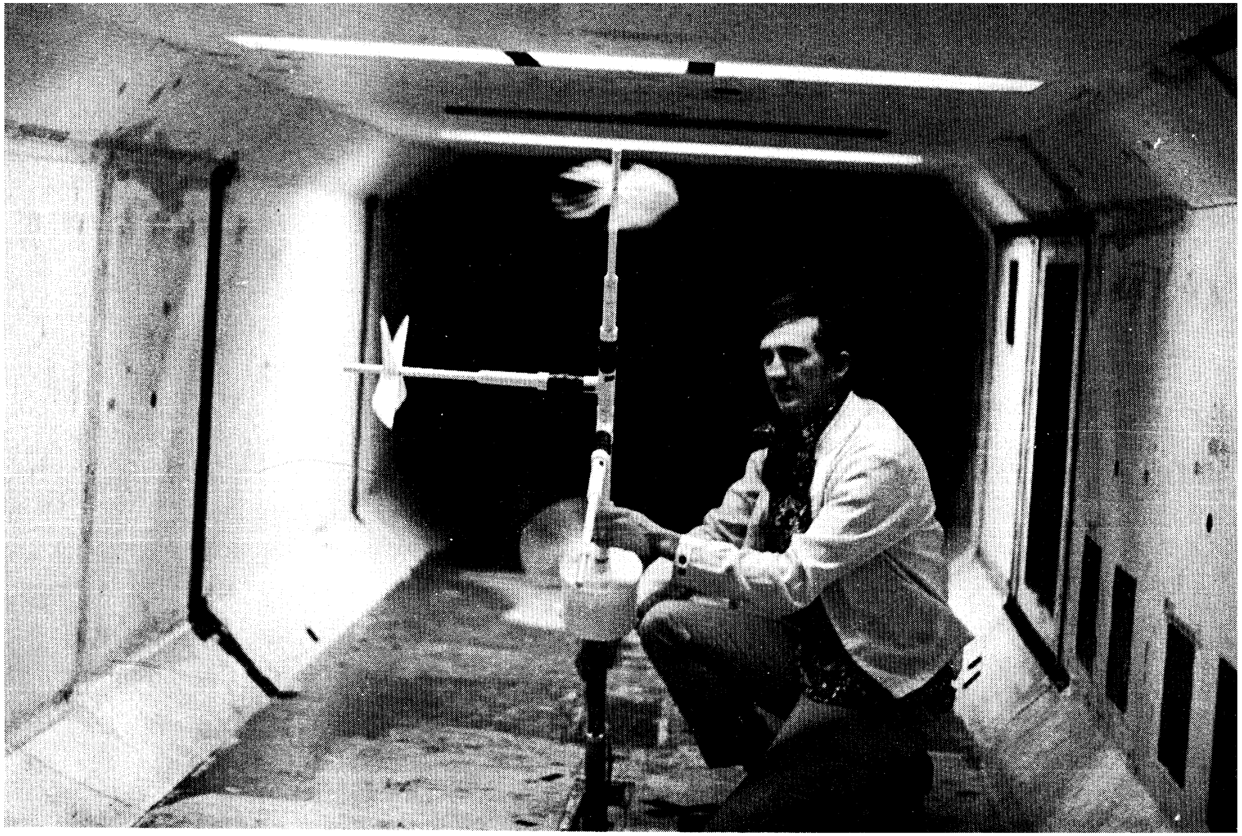

Figure 3.2.1
Orthogonal UVW in AE wind tunnel.

Hence, guided by the fact that the instantaneous wind vector in a turbulent flow field remote from any major obstructions seldom lies outside an angular space of 30° in any direction from the mean, we decided on a sensor aspect angle of 30° (i.e., the axes of the three propellers are located on a conical surface having a solid angle of 30° ($\eta = 15^\circ$)). This choice would at the same time satisfy (a) for a wide span of wind directions (see Figure 3.1.2), while, of course, the highest degree of accuracy would be obtained only by heading the sensor into the mean wind direction. Figures 3.2.2a and b show the 30° UVW sensor. Correspondingly, the Orthogonal UVW sensor has its axes effectively on a cone of 110° solid angle.

The tests of the two described systems were performed in the already mentioned AE wind tunnel. By means of the turning mechanism shown on Figure 3.2.3 it was possible to tilt the system up to 45°, and in all tilted positions a 360 degree rotation could be performed. The hereby defined elevation (El) and azimuth (Az) angles are known relatively within less than 0.5°. Hence the true alignment of the sensor in the tunnel at each step is known, except for basic reference angles.

Referring to Figure 3.1.1, we notice that the probe system and the reference system are firmly attached to each other by the construction of the sensor. But since the sensor is attached to the turning mechanism, subject to some unknown offset angle, we have found it advantageous to introduce a new reference system. It is simply the old one rotated about the sensor axis in a

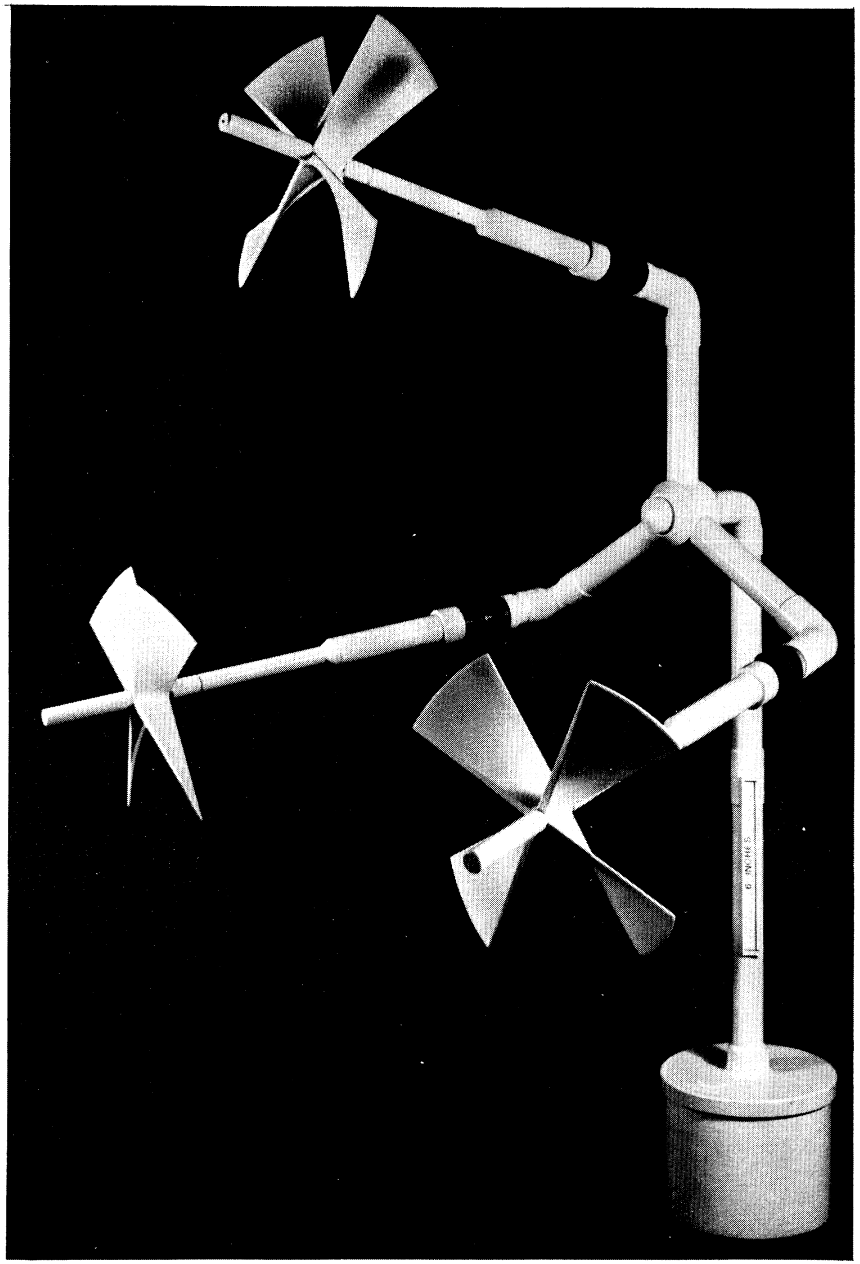

Figure 3.2.2a

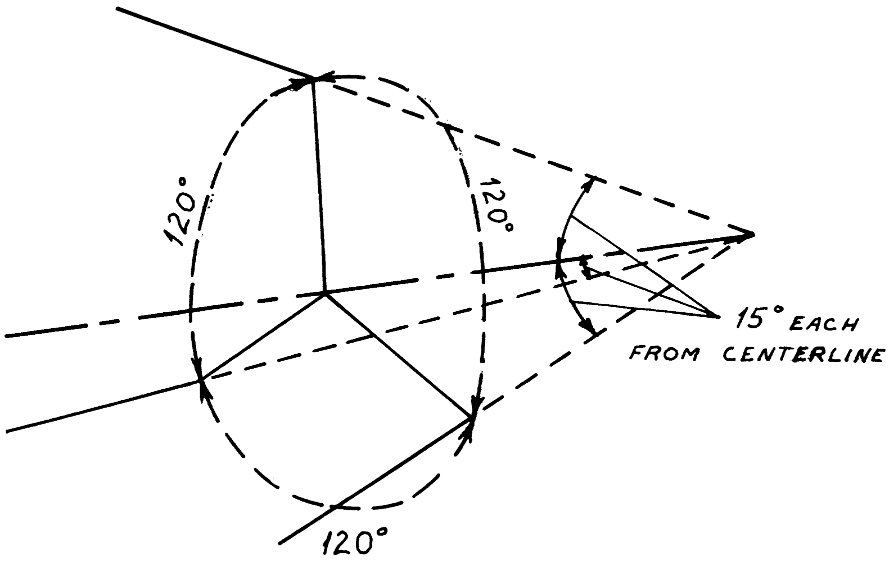

Figure 3.2.2b

The 30° UVW sensor.

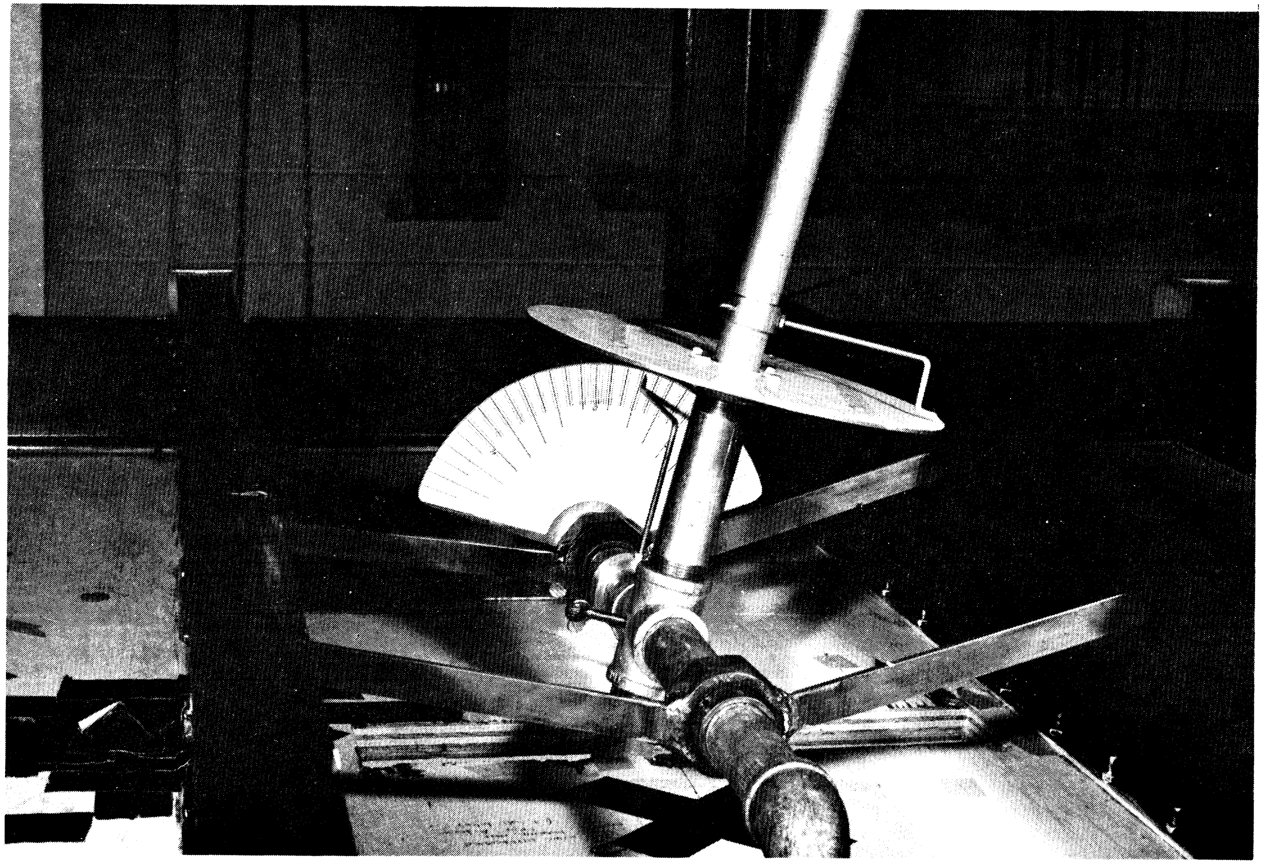

Figure 3.2.3
Mounting device for measurement of angular response of a three-propeller sensor.

counter clockwise direction, when facing the front of the sensor (ϕ).

For a total description of the sensor alignment in the tunnel, we finally introduce a so-called fixed azimuth angle (Az_f). This angle is defined in the fixed tunnel coordinate system--by the tunnel floor (UV-plane) and the flow direction (U-axis). It is the angle between the UW-plane and the vertical plane containing the W-axis of the tunnel system and the W_{r2}-axis of the redefined reference system.

In order to clarify all coordinate systems involved, Figures 3.2.4 and 3.2.5 are presented.

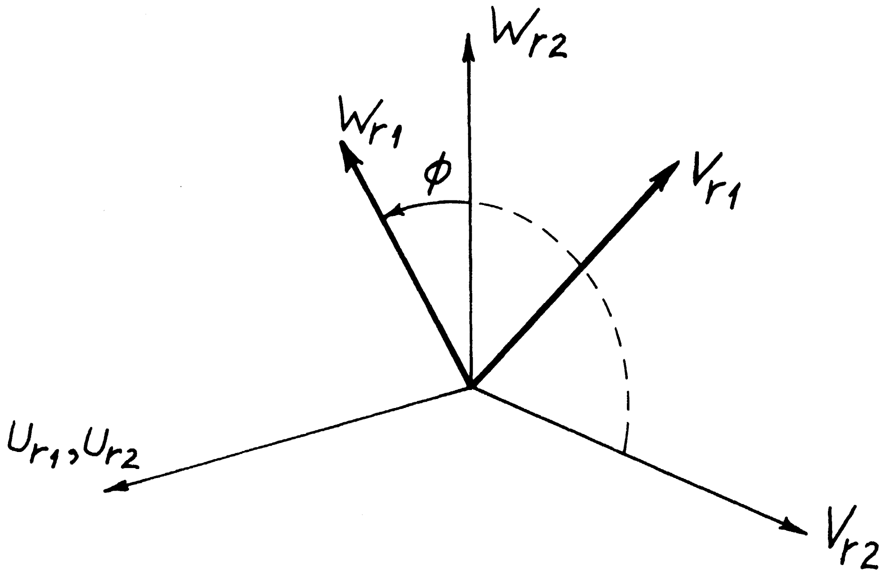

Figure 3.2.4
Reference coordinate systems (Ref. 1 and Ref. 2).

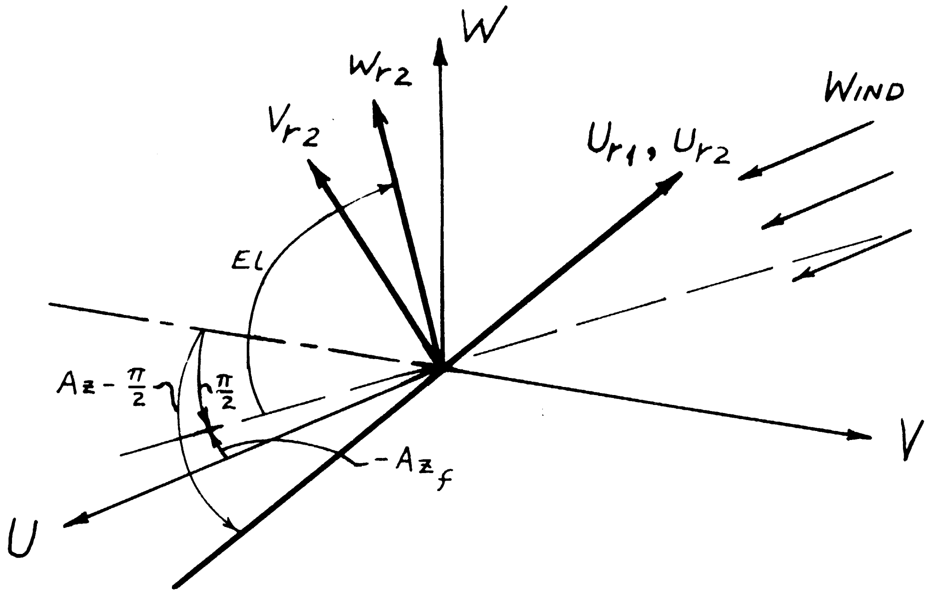

Figure 3.2.5
Wind tunnel coordinate system versus reference system (Ref. 2).

The experiments were conducted in the following manner.

1) All applied propellers were calibrated together with their dc-tachometers in axial flow, yielding linear relationships between magnitude of axial flow and tachometer output in volts.

2) The AE tunnel was set at a constant speed and the tachometer outputs were measured at each alignment of the sensor (Az, El). For each Az elevation angle setting, the azimuth settings were changed in constant increments from stall of U-propeller to stall of V-propeller. (The tunnel speed was usually changed from one setting of El to another, but never during changes of Az at any chosen El.) Since we were only interested in learning the sensor ability

to measure in three dimensions, we did not make any accurate measurements of the exact tunnel speed at the position of the sensor but monitored only the tunnel inlet speed by means of the venturimeter naturally composed by the contraction section (15:1) immediately upstream of the test section. At very low tunnel speeds this gives very inaccurate results due to the very small differential pressures involved. But at tunnel speeds larger than 10 m/s, this should yield acceptable results for the speed in the test section; but still only a fair approximation of the speed at the sensor.

All measurements (voltages versus Az and El) were fed into a computer programmed to solve the earlier mentioned equations and finally to print out the velocity components in the fixed tunnel coordinate system. (A listing of the program is filed as Appendix A to this report.) Tables 3.2.1a-1d, 3.2.2 and 3.2.3a-3b contain the computed results. The results are referred to a coordinate system slightly rotated in comparison to the tunnel system.

Tables 3.2.1a through 3.2.3b should be self explanatory, for most part. The first six columns give wind velocity components in voltage outputs and meters per second. The column denoted "Velocity" is the magnitude of the measured velocity as it is sensed by the fastest running propeller. By using this estimate, we should improve the overall accuracy, since the angular response function is most accurate for small angles of attack. The next column denoted "Error" indicates the maximum deviation of the

Propeller output volts			Wind components m/sec			Velocity m/sec	Error %	Az degree	
U	V	W	U	V	W				
0.0	0.540	0.0	8.378	0.076	0.180	8.387		-89.5	3
0.066	0.531	0.0	8.491	-0.074	0.183	8.500	0.16	-79.5	5
0.130	0.500	0.0	8.510	0.028	0.183	8.517	-0.07	-69.5	6
0.170	0.480	0.0	8.619	-0.037	0.185	8.626	0.02	-64.5	7
0.201	0.443	0.0	8.476	-0.021	0.182	8.482	-0.01	-59.5	8
0.234	0.414	0.0	8.542	0.062	0.184	8.548	0.03	-54.5	9
0.273	0.374	0.0	8.579	0.058	0.184	8.583	-0.02	-49.5	12
0.313	0.328	0.0	8.543	0.044	0.184	8.547	-0.02	-44.5	8
0.355	0.284	0.0	8.535	0.023	0.184	8.538	-0.02	-39.5	12
0.392	0.243	0.0	8.493	0.018	0.183	8.496	0.02	-34.5	9
0.426	0.210	0.0	8.554	0.075	0.184	8.557	0.04	-29.5	7
0.452	0.179	0.0	8.587	0.177	0.185	8.591	0.02	-24.5	7
0.475	0.137	0.0	8.550	0.094	0.184	8.552	-0.07	-19.5	6
0.493	0.103	0.0	8.574	0.152	0.184	8.577	-0.06	-14.5	6
0.507	0.068	0.0	8.572	0.169	0.184	8.575	0.14	-9.5	5
0.516	0.027	0.0	8.526	-0.015	0.183	8.528		-4.5	4
0.518	0.0	0.0	8.517	0.069	0.183	8.519		0.5	3
accumulated mean			8.532	0.053	0.183				
accumulated deviation			0.053	0.068	0.001				

Table 3.2.1a

Orthogonal UVW results with $Az_f = 0.0^\circ$

elevation of Z-axis = 91.2°
aspect angle = 109.4°
no probe system rotation

Propeller output volts			Wind components m/sec			Velocity m/sec	Error %	Az degree	
U	V	W	U	V	W				
0.0	0.520	0.088	8.486	0.076	0.235	8.496	-0.05	-89.5	6
0.025	0.519	0.088	8.504	0.147	0.240	8.514	-0.05	-84.5	6
0.060	0.511	0.088	8.525	0.019	0.245	8.533	-0.06	-79.5	6
0.092	0.498	0.088	8.526	0.024	0.245	8.534	-0.06	-74.5	6
0.122	0.484	0.088	8.553	0.111	0.252	8.561	0.02	-69.5	7
0.160	0.461	0.088	8.597	0.041	0.263	8.604	0.03	-64.5	7
0.193	0.430	0.088	8.574	0.041	0.258	8.580	-0.02	-59.5	8
0.221	0.398	0.088	8.541	0.143	0.249	8.548	0.03	-54.5	9
0.258	0.357	0.088	8.549	0.105	0.251	8.554	0.02	-49.5	11
0.297	0.318	0.088	8.595	0.103	0.263	8.600	-0.01	-44.5	8
0.334	0.278	0.088	8.571	0.115	0.257	8.575	0.02	-39.5	11
0.370	0.234	0.088	8.463	0.045	0.230	8.466	-0.01	-34.5	10
0.401	0.207	0.088	8.534	0.176	0.248	8.539	-0.02	-29.5	8
0.469	0.099	0.088	8.515	0.154	0.243	8.519	-0.06	-14.5	6
0.480	0.080	0.088	8.561	0.471	0.254	8.576	-0.06	-9.5	6
0.490	0.029	0.088	8.510	0.056	0.242	8.513	-0.05	-4.5	6
0.493	0.0	0.088	8.520	0.067	0.244	8.523	-0.05	0.5	6
accumulated mean			8.537	0.111	0.248				
accumulated deviation			0.035	0.101	0.009				

Table 3.2.1b

Orthogonal UVW results with $Az_f = 0.0^\circ$

elevation of Z-axis = 106.2°
aspect angle = 109.4°
no probe system rotation

Propeller output volts			Wind components m/sec			Velocity m/sec	Error %	Az degree	
U	V	W	U	V	W				
0.0	0.448	0.188	8.433	0.069	0.245	8.441	0.03	-89.5	7
0.030	0.442	0.188	8.399	-0.068	0.228	8.406	0.04	-84.5	7
0.063	0.436	0.188	8.454	-0.211	0.261	8.474	-0.01	-79.5	8
0.089	0.423	0.188	8.465	-0.151	0.262	8.473	-0.02	-74.5	8
0.117	0.408	0.188	8.505	-0.101	0.282	8.513	0.01	-69.5	9
0.145	0.383	0.188	8.472	-0.076	0.265	8.478	0.02	-64.5	9
0.189	0.360	0.188	8.699	-0.275	0.382	8.712	-0.01	-59.5	10
0.201	0.324	0.188	8.439	-0.061	0.249	8.444	-0.01	-54.5	10
0.229	0.298	0.188	8.497	-0.007	0.278	8.501	0.01	-49.5	9
0.260	0.260	0.188	8.441	-0.094	0.250	8.445	-0.01	-44.5	8
0.290	0.232	0.188	8.475	-0.070	0.267	8.479	0.02	-39.5	9
0.319	0.200	0.188	8.446	-0.090	0.253	8.450	-0.01	-34.5	10
0.348	0.182	0.188	8.597	0.084	0.330	8.603	-0.01	-29.5	10
0.370	0.146	0.188	8.505	0.035	0.282	8.509	0.02	-24.5	9
0.391	0.115	0.188	8.508	0.049	0.284	8.512	0.01	-19.5	9
0.408	0.084	0.188	8.516	0.054	0.288	8.520	-0.02	-14.5	8
0.419	0.056	0.188	8.515	0.096	0.287	8.519	-0.01	-9.5	8
0.428	0.016	0.188	8.516	-0.195	0.288	8.522	0.03	-4.5	7
0.430	0.0	0.188	8.535	0.060	0.298	8.540	0.03	0.5	7
accumulated mean			8.496	-0.050	0.278				
accumulated deivation			0.065	0.105	0.033				

Table 3.2.1c

Orthogonal UVW results with $Az_f = 0.0^\circ$
elevation of Z-axis = 121.2°
aspect angle = 109.4°
no probe system rotation

Propeller output volts			Wind components m/sec			Velocity m/sec	Error %	Az degree	
U	V	W	U	V	W				
0.0	0.340	0.300	8.617	0.059	0.307	8.627	0.01	-89.5	11
0.0	0.338	0.300	8.571	0.595	0.269	8.600	0.01	-84.5	11
0.044	0.324	0.300	8.519	-0.005	0.240	8.525	0.01	-79.5	7
0.090	0.310	0.300	8.628	0.029	0.315	8.636	-0.02	-69.5	10
0.111	0.292	0.300	8.572	0.072	0.277	8.579	0.01	-64.5	11
0.132	0.277	0.300	8.574	0.137	0.279	8.581	-0.02	-59.5	10
0.158	0.253	0.300	8.543	0.045	0.258	8.548	-0.01	-54.5	10
0.181	0.230	0.300	8.522	-0.004	0.244	8.527	-0.01	-49.5	10
0.200	0.212	0.300	8.539	0.056	0.254	8.544	0.02	-44.5	9
0.218	0.200	0.300	8.624	0.216	0.311	8.633	0.02	-39.5	9
0.237	0.178	0.300	8.626	0.240	0.314	8.635	-0.01	-34.5	10
0.254	0.147	0.300	8.540	0.147	0.257	8.546	-0.02	-29.5	10
0.270	0.120	0.300	8.515	0.116	0.238	8.519	0.01	-24.5	11
0.288	0.100	0.300	8.596	0.190	0.294	8.603	-0.02	-19.5	10
0.300	0.080	0.300	8.617	0.295	0.306	8.628	0.02	-14.5	9
0.310	0.052	0.300	8.595	0.220	0.292	8.604	-0.02	-9.5	8
0.317	0.020	0.300	8.581	0.004	0.284	8.587	-0.02	-4.5	10
0.320	0.0	0.300	8.603	0.049	0.298	8.610	0.01	0.5	11
accumulated mean			8.577	0.137	0.280				
acculated deviation			0.038	0.142	0.026				

Table 3.2.1d

Orthogonal UVW results with $Az_{£} = 0.0^{\circ}$
elevation of Z-axis = 136.2°
aspect angle = 109.4°
no probe system rotation

Propeller output volts			Wind Components m/sec			Velocity m/sec	Error %	Az degree	
U	V	W	U	V	W				
0.0	0.128	0.070	6.410	0.294	-0.523	6.438	0.48	-68.5	4
0.034	0.147	0.091	5.306	-0.105	-0.137	5.309	0.01	-63.5	4
0.075	0.198	0.133	5.506	-0.022	-0.106	5.507	0.15	-53.5	4
0.128	0.254	0.181	5.229	-0.292	0.070	5.238	0.05	-43.5	7
0.170	0.300	0.233	5.633	-0.029	-0.049	5.633	-0.03	-33.5	10
0.225	0.330	0.277	5.648	-0.049	0.059	5.648	-0.02	-23.5	18
0.273	0.345	0.310	5.693	-0.017	-0.060	5.693	-0.01	-13.5	12
0.315	0.351	0.333	5.778	-0.061	-0.029	5.778	0.07	-3.5	5
0.339	0.338	0.339	5.810	-0.093	0.011	5.810	0.01	6.5	7
0.347	0.311	0.331	5.826	-0.064	-0.032	5.826	-0.01	16.5	8
0.343	0.275	0.312	5.824	0.077	0.032	5.825	-0.01	26.5	16
0.329	0.222	0.282	5.917	0.047	0.025	5.917	-0.01	36.5	16
0.290	0.167	0.233	5.737	0.153	-0.072	5.740	-0.03	46.5	10
0.248	0.123	0.183	5.682	0.244	0.010	5.687	0.01	56.5	6
0.192	0.074	0.136	5.634	0.239	-0.078	5.639	-0.06	66.5	5
0.142	0.034	0.089	5.260	0.350	0.155	5.274	0.02	76.5	4
0.124	0.0	0.069	6.373	0.017	-0.180	6.376	-0.03	81.5	4
accumulated mean			5.721	0.041	-0.053				
accumulated deviation			0.313	0.162	0.142				

Table 3.2.2

30° UVW results with $Az_f = -5.0^{\circ}$

elevation of Z-axis = 94.0°
aspect angle = 29.4°
probe system rotation = 1.5° counter-clockwise

Propeller output volts			Wind components m/sec			Velocity m/sec	Error %	Az degree	
U	V	W	U	V	W				
0.0	0.344	0.248	18.156	-0.068	0.418	18.161	0.05	-77.4	4
0.052	0.418	0.317	18.773	0.198	0.520	18.782	-0.03	-72.4	4
0.193	0.550	0.460	17.960	-0.122	0.179	17.961	-0.03	-62.4	5
0.331	0.708	0.621	18.572	0.108	0.038	18.572	-0.11	-52.4	4
0.473	0.852	0.790	18.494	0.081	0.048	18.494	0.02	-42.4	9
0.626	0.957	0.937	18.353	-0.112	0.074	18.353	0.02	-32.4	9
0.779	1.014	1.039	18.469	-0.085	-0.034	18.469	0.01	-22.4	23
0.908	1.028	1.108	18.582	-0.065	-0.130	18.582	0.01	-12.4	11
0.988	0.996	1.128	18.522	-0.026	-0.026	18.522	-0.10	-2.4	6
1.029	0.920	1.109	18.683	-0.079	-0.157	18.684	-0.01	7.6	12
1.025	0.303	1.045	18.660	0.069	-0.025	18.660	-0.02	17.6	24
0.974	0.653	0.943	18.539	0.179	0.044	18.540	0.01	27.6	11
0.879	0.494	0.800	19.061	-0.201	-0.262	19.064	-0.02	37.6	10
0.745	0.365	0.632	18.523	0.296	0.036	18.525	-0.31	47.6	4
0.586	0.214	0.468	18.469	0.174	0.187	18.470	-0.04	57.6	5
0.438	0.087	0.325	17.715	0.478	0.263	17.723	0.31	67.6	3
0.377	0.0	0.252	19.747	-0.199	0.159	19.749	0.01	72.6	5
accumulated mean			18.546	0.037	0.078				
accumulated deviation			0.424	0.180	0.192				

Table 3.2.3a

30° UVW results with $Az_r = 2.0^\circ$

elevation of Z-axis = 106.2°
aspect angle = 29.4°
probe system rotation = -2.2° counter-clockwise
relative accuracy = 99.99%

Propeller output volts U	Propeller output volts V	Propeller output volts W	Wind components m/sec U	Wind components m/sec V	Wind components m/sec W	Velocity m/sec	Error %	Az degree	
0.0	0.344	0.248	18.169	-0.068	0.423	18.174		-77.4	3
0.052	0.418	0.317	18.789	0.199	0.525	18.797	0.22	-72.4	3
0.191	0.550	0.460	17.971	-0.121	0.185	17.973	0.10	-62.4	4
0.331	0.708	0.521	18.572	0.108	0.038	18.572	-0.11	-52.4	4
0.473	0.852	0.790	18.486	0.077	0.034	18.486	-0.10	-42.4	6
0.626	0.957	0.937	18.369	-0.122	0.089	18.370	-0.19	-32.4	6
0.779	1.014	1.039	18.480	-0.104	-0.025	18.481	-0.13	-22.4	16
0.908	1.028	1.108	18.593	-0.087	-0.129	18.593	-0.11	-12.4	8
0.988	0.996	1.128	18.508	-0.042	-0.284	18.510	2.28	-2.4	3
1.029	0.920	1.109	18.697	-0.054	-0.152	18.698	-0.16	7.6	8
1.025	0.803	1.045	18.648	0.049	-0.037	18.648	0.13	17.6	17
0.974	0.653	0.943	18.551	0.189	0.048	18.552	-0.10	27.6	8
0.879	0.494	0.800	19.090	-0.177	-0.347	19.094	-0.72	37.6	4
0.745	0.365	0.632	18.523	0.296	0.036	18.525	-0.31	47.6	4
0.586	0.214	0.468	18.484	0.172	0.197	18.486	0.17	57.6	4
0.438	0.087	0.325	17.715	0.478	0.263	17.723	0.31	67.6	3
0.377	0.0	0.252	19.744	-0.199	0.157	19.745	-0.08	72.6	4
accumulated mean			18.552	0.035	0.060				
accumulated deviation			0.423	0.180	0.219				

Table 3.2.3b

30° UVW results with $Az_f = 2.0^{\circ}$

elevation of Z-axis $= 106.2^{\circ}$
aspect angle $= 29.4^{\circ}$
probe system rotation $= -2.2^{\circ}$ counter-clockwise
relative accuracy = 99.90%

magnitude of speed as calculated from all three propellers. The last unlabeled column displays the necessary number of iterations to achieve the listed accuracies. We notice that these numbers increase as the sensor approaches a symmetrical alignment in the tunnel. This is evident since all iterations are initiated by an assumed axial flow toward the fastest running propeller. Tables 3.2.3a and 3.2.3b are included to indicate the effect of diminishing the relative accuracy of the iteration algorithm (from 99.99% to 99.90%). The effect seems insignificant in terms of achieved overall accuracy although the amount of computation time on the average decreases 25%.

As mentioned already, the listed U, V and W-components are referred to a coordinate system approximately aligned with the fixed tunnel system. The accumulated mean of all components indicates,however, some offset in the alignments. Some of these offsets are due to inaccuracies in the azimuth and elevation settings at the different sensor positions, and some are due to inaccuracy in the reference settings of the azimuth and elevation angles. The latter source of errors can be eliminated by rotating the coordinate system. This has been done to some extent, and in most cases the accumulated means are acceptably low. This optimizing process was, however, not carried out all the way through, since it had very little impact on the accumulated deviations in each separate experiment.

As expected, the measurements by means of the 30° UVW sensor are very sensitive to the aspect angle η. Also, they are extremely sensitive to even small differences in η for each propeller. Since a simple geometric consideration concerning the 30° UVW revealed about a one degree offset of one propeller axis, we decided to use an average angle $\bar{\eta}$, computed as the angle yielding a minimum of variance on all three velocity components in the experiments dealt with in Tables 3.2.3a-3b. We found $\bar{\eta} = 14.7^{\circ}$. Applying the same reasoning on the measurements of Table 3.2.2, however, we did not find a minimum between 14° and 15°, although $\bar{\eta} = 14^{\circ}$ was better than $\bar{\eta} = 15^{\circ}$. Of course, the proper way to deal with η is to perform a complete geometric survey of the sensor and calculate an accurate $\bar{\eta}$. Unfortunately, we cannot do this with an acceptable degree of accuracy ($\pm 0.1^{\circ}$) without possessing an optical measuring stand of some kind. On the other hand, by simple means, the three η angles can be brought quite close to each other, leaving the mentioned otimizing procedure to be acceptable.

In order to reach some kind of quantitative measure of the sensor fitness for three-dimensional velocity measurements, we have in Table 3.2.4 listed the velocity components and their relative deviations, calculated at different elevation angles and different spans of azimuth angles. From this table we may conclude that both systems are working with reasonable accuracy over equal azimuth spans. As expected, the overall accuracy decreases with a widening of the span, but even at the widest possible span (150° for 30° UVW) the inaccuracy is not prohibitively large. The seemingly large inaccuracy obtained at

nsor	El degrees	ΔAz degrees	Tunnel speed* m/s	U-comp.		V-comp.		W-comp.	
				mean m/s	S.D./U	mean m/s	S.D./U	mean m/s	S.D./U
0° VW	94.0	±75.0	6.0	5.72	.054	.04	.028	-.05	.024
	94.0	±60.0	6.0	5.69	.030	.01	.025	-.02	.009
	94.0	±50.0	6.0	5.71	.030	-.01	.023	.00	.009
	94.0	±30.0	6.0	5.79	.013	-.02	.010	.00	.007
	106.2	±75.0	18.6	18.55	.023	.04	.010	.08	.010
	106.2	±60.0	18.6	18.53	.012	.02	.008	-.02	.006
	106.2	±50.0	18.6	18.59	.009	.01	.008	-.04	.005
	106.2	±30.0	18.6	18.54	.005	-.02	.005	-.04	.004
thonal VW	91.2	±45.0	9.2	8.53	.006	.05	.008	.18	.000
	91.2	±30.0	9.2	8.55	.005	.06	.008	.18	.000
	106.2	±45.0	9.2	8.53	.004	.11	.012	.25	.001
	106.2	±30.0	9.2	8.55	.005	.14	.013	.25	.001
	121.2	±45.0	9.2	8.50	.007	-.05	.013	.28	.004
	121.2	±30.0	9.2	8.51	.008	-.04	.012	.28	.004

*Speed measured at Tunnel inlet by means of pressure drop across the contraction section. The differential pressure was measured rather inaccurately.

Table 3.2.4

Reference coordinate systems (Ref. 1 and Ref. 2).

the lowest tunnel speed is probably not entirely due to the sensor, since the output voltages from the tachometer at this speed are rather low, yielding a relatively high percentage error.

As stated earlier in this report (Chapter 2.1), we have encountered some indication that the pitchfactor of the propellers (γ_T) is temperature dependent. It should therefore be mentioned that the 30° UVW experiments were performed at an ambient temperature of $23^\circ C$, while the individual propellers were calibrated at $31^\circ C$. This temperature difference of $8^\circ C$ yields an increase in γ_T of approximately 1.6%, if the temperature dependence is to be believed. All calculations concerning these experiments include this 1.6% temperature correction. The improved agreement between venturimeter readings and sensor readings does not contradict the assumed temperature dependence (see Appendix B).

The described experiments do not prove the 30° UVW is significantly better than the Orthogonal UVW. On the other hand, they do indicate that either of the sensors is working satisfactorily as a three-dimensional sensor. But since the azimuth span of the 30° UVW is much wider than the span of the Orthogonal UVW, it seems fair to state that the 30° UVW is to be preferred in practice. One must, however, bear in mind that the tolerances in manufacturing of the 30° UVW must be kept very small to achieve good measurements. It is our experience that the aspect angle of the sensor should be known within $\pm 0.1^\circ$, and that all propeller axes should have slopes toward the axis of the sensor with a deviation of not more than $\pm 0.1^\circ$.

Conclusions

Commerically available helicoid propeller sensors have been investigated with the specific purpose of improving their applicability to wind measurement. Some recommendations concerning their suitability for turbulence measurements are made, but any conclusive statement is not possible because field tests were not conducted. It can, however, be concluded that measurements in a turbulent flow field by means of propeller sensors, where any of the propellers are attacked at small angles toward the propeller plane will be erroneous, since those particular propellers will stand still during a not-insignificant part of the recording time.

Helicoid propellers are found to have an angular response function different from the cosine function. Their actual response differs from one propeller type to another; but for one type we have displayed experimental evidence suggesting a function independent of speed and individual propellers.

By applying the experience and knowledge gained by the preliminary investigation, we have developed a three-propeller sensor which has proved promising for three-dimensional velocity measurements. The sensor has still to be tried out in a turbulent wind field, so a final evaluation of its suitability for three-dimensional turbulence measurements must await these tests.

Appendix A

Computer program for U, V, W analysis

```
      UVW-ANALYSES
*********
       DIMENSION  SF(3),SV(3),FO(3),VO(3),E(3,100),AN(3,100),F(3,100),
     1FI(5),U(100),CS(3),NI(3),NDD(3),NP(3),PCT(100),T(100),NIT(100),
     2SU1(3),SU2(3),UN(3),DUM(3)
      DATA SU1,SU2,UN,DUM/12*0./
*********
*********
      RA=3.14159/180.
      READ(5,100) TANG,OMEG,RADI,DT,NTOT,NSEQ,DAZF,DAZ,DEL
  100 FORMAT(4F10.4,2I10,3F5.1)
      READ(5,101) SF,FO,SV,VO
  101 FORMAT(6F10.4)
      TNG=TANG*RA
      OMG=OMEG*RA
      D3=SIN(OMG)
      D4=COS(OMG)
      TANG=TANG*2.
      TNGO=ATAN(SQRT(2.))
      D0=3.*COS(TNG)*SIN(TNG)
      D1=(COS(TNGO)*SIN(TNG)+2.*SIN(TNGO)*COS(TNG))/D0
      D2=SIN(TNG-TNGO)/D0
      N1=NSEQ
      NSER=-N1
      IF(NSEQ.GE.NTOT) NSER=-NTOT
      DO 1020 I=1,3
      SV(I)=SV(I)*RADI
 1020 CONTINUE
*********
 1009 CONTINUE
      NTOT=NTOT-NSEQ
      NSER=NSER+N1
      IF(NTOT.GT.0) GO TO 1000
      N1=NTOT+NSEQ
      IF(N1.LE.0) STOP
 1000 CONTINUE
*********
      READ(5,102)((E(I,K),I=1,3),(AN(I,K),I=1,3),K=1,N1)
  102 FORMAT(6F10.4)
*****************************************************************************
      DO 1001 J=1,N1
      DO 1002 I=1,3
      F(I,J)=SF(I)*ABS(E(I,J))+FO(I)
      IF(E(I,J).LT.0.) F(I,J)=-F(I,J)
      CS(I)=1.0
      NI(I)=I
 1002 CONTINUE
*********
      GN=ABS(F(1,J))
      DO 1003 I=2,3
      IF(ABS(F(I,J)).LT.GN) GO TO 1003
      GN=ABS(F(I,J))
      NI(1)=I
      IF(I .NE. 2) GO TO 1023
      NI(2)=1
```

```
      NI(3)=3
      GO TO 1003
 1023 CONTINUE
      NI(2)=2
      NI(3)=1
 1003 CONTINUE
********* ITERATION BEGINS
      CS1=1.0
      DO 1007 ITR=1,100
      I1=NI(1)
      RL1=RL(CS(I1))
      RP(I1)=CS(I1)*RL1
      F1(I1)=F(I1,J)*SV(I1)+VO(I1)*RP(I1)
      F2=F1(I1)
      DO 1004 I=2,3
      I1=NI(I)
      ARG=CS(I1)*CS1
      RDD(I1)=RD(ARG)
      RP(I1)=ARG*RDD(I1)
      F1(I1)=F(I1,J)*SV(I1)+VO(I1)*RP(I1)
      RDD(I1)=RL1/RDD(I1)
      CS(I1)=F1(I1)*RDD(I1)/F2
 1004 CONTINUE
*********
      I1=NI(1)
      I2=NI(2)
      I3=NI(3)
      IF(I1 .EQ. 3) GO TO 1024
      CSN=(CS(I2)-1.)*(1.+CS(I2)-2.*CS(I3))
      IF(I1.EQ.2) CSN=-CSN
      GO TO 1025
 1024 CONTINUE
      CSN=(CS(I2)-CS(I3))*(CS(I2)+CS(I3)-2.)
 1025 CONTINUE
      CS(I1)=1.5*SIN(2.*TNG)/SQRT((1.+CS(I2)+CS(I3))**2+3.*COS(TNG)**
     11.-2.*(CS(I2)+CS(I3))+(CS(I2)-CS(I3))**2))
*********
      IF(ABS(CS1-CS(I1)).LT.10.**(-4)*CS(I1)) GO TO 1008
      CS1=CS(I1)
      IF(ITR.GE.25) GO TO 1008
      GO TO 1007
*********END OF ITERATION
 1008 CONTINUE
      CS(I2)=CS(I2)*CS(I1)
      CS(I3)=CS(I3)*CS(I1)
      U1=F1(I1)/RP(I1)
      U2=U1
      U3=U1
      IF(ABS(RP(I2)).GT.10.**(-5)) U2=F1(I2)/RP(I2)
      IF(ABS(RP(I3)).GT.10.**(-5)) U3=F1(I3)/RP(I3)
      PCT(J)=(U1-U2)/U1*100.
      IF(ABS(U1-U3).GT.ABS(U1-U2)) PCT(J)=(U1-U3)/U1*100.
      U(J)=U1
      T(J)=FLOAT(NSER+J)*DT
      COUN=NSER+J
********* VELOCITY VECTOR,PROBE SYSTEM
      F1(1)=(CS(1)+CS(2)+CS(3))/3./COS(TNG)*U1
```

```
      F1(2)=(CS(2)-CS(1))/SQRT(3.)/SIN(TNG)*U1
      F1(3)=(2.*CS(3)-(CS(1)+CS(2)))/3./SIN(TNG)*U1
      F1(4)=F1(2)*D4-F1(3)*D3
      F1(5)=F1(2)*D3+F1(3)*D4
      F1(2)=F1(4)
      F1(3)=-F1(5)
      NIT(J)=ITE
C********* POSITION OF FIX. COOR. SYSTEM
      IF(J.NE.1.OR.NSER.NE.0.) GO TO 1010
      AZF1=AN(1,J)*RA
      AZ1=AN(2,J)*RA
      EL1=AN(3,J)*RA
 1010 CONTINUE
      IF(ABS(AN(1,J)).GT.10.**(-5))    AZF1=AN(1,J)*RA
      IF(ABS(AN(2,J)).GT.10.**(-5))    AZ1 =AN(2,J)*RA
      IF(ABS(AN(3,J)).GT.10.**(-5))    EL1 =AN(3,J)*RA
      AN(1,J)=AZF1/RA+DAZF
      AN(2,J)=AZ1/RA+DAZ-AN(1,J)
      AN(3,J)=EL1/RA+DEL
      AZ=AN(2,J)*RA
      AZF=AN(1,J)*RA
      EL=AN(3,J)*RA
C********* VELOCITY VECTOR, FIX.SYSTEM
      F(1,J)=F1(1)*(COS(AZF)*COS(AZ)*SIN(EL)-SIN(AZF)*SIN(AZ))
     1        -F1(2)*(COS(AZF)*SIN(AZ)*SIN(EL)+SIN(AZF)*COS(AZ))
     2        +F1(3)*(COS(AZF)*COS(EL))
      F(2,J)=F1(1)*(SIN(AZF)*COS(AZ)*SIN(EL)+COS(AZF)*SIN(AZ))
     1        -F1(2)*(SIN(AZF)*SIN(AZ)*SIN(EL)-COS(AZF)*COS(AZ))
     2        +F1(3)*(SIN(AZF)*COS(EL))
      F(3,J)=-F1(1)*COS(AZ)*COS(EL)
     1         +F1(2)*SIN(AZ)*COS(EL)
     2         +F1(3)*SIN(EL)
      GO TO 1001
 1007 CONTINUE
 1001 CONTINUE
C*****************************************************************
      WRITE(6,103) (T(J),(E(I,J),I=1,3),(F(I,J),I=1,3),U(J),PCT(J),(AN(I,
     1J),I=1,3),NIT(J),J=1,N1)
  103 FORMAT('1UVW-ANALYSES'/'0 REC.TIME    U-PROP.    V-PROP.    W-PROP.
     1 U-COMP.    V-COMP.    W-COMP.   VELOCITY ERROR,PCT AZIMUT F. AZIMUT
     2V. Z-AX.ELV.'/'          SEC        VOLT       VOLT       VOLT     M/SEC
     3    M/SEC      M/SEC      M/SEC    PERCENT     DEGREE     DEGREE     DEG
     4REE'//,(F10.3,7F10.3,F10.2,3F10.1,I10/))
      DO 1021 J=1,N1
      DO 1021 I=1,3
      SU1(I)=SU1(I)+F(I,J)
      SU2(I)=SU2(I)+F(I,J)**2
 1021 CONTINUE
      DO 1022 I=1,3
      UM(I)=SU1(I)/COUN
      DUM(I)=SQRT(SU2(I)/COUN-UM(I)**2)
 1022 CONTINUE
      WRITE(6,105)  (UM(I),I=1,3),(DUM(J),J=1,3)
  105 FORMAT('0ACCUMULATED MEAN',23X,3F10.3/' ACCUMULATED DEVIATION',18X
     1,3F10.3)
      WRITE(6,104) TANG,OMEG
  104 FORMAT('0ASPECT ANGLE OF UVW =' ,F5.1,' DEGREES'/' PROBE SYSTEM RO
```

```
1TATED ',F5.1,' DEGREES COUNTER CLOCKWISE')
 GO TO 1009
 END
```

```
 FUNCTION RD (ANG)
 A0=   .6286
 A2=  1.2636
 A4= -5.3595
 A6= 12.6617
 A8=-12.8128
 A10= 4.6182
 CS=ANG
 RD=A0+A2*CS**2+A4*CS**4+A6*CS**6+A8*CS**8+A10*CS**10
 RETURN
 END
```

Appendix B

A Note on the Apparent Temperature Dependence of the Pitchfactor

Table 2.1.2 of this report seems to reveal some evidence of changes in propeller calibrations with changes in ambient temperature. In order to collect more data on this matter, we decided to perform a calibration of propeller "Ref", at an ambient temperature significantly lower than stated in Table 2.1.2.

The temperature during the calibration run was approximately 11°C, which should give us, according to earlier findings, an increase in pitchfactor of approximately 4%. We obtain, however, the following results:

$$\gamma_T = .419, \text{ S.D.} = 0.001,$$

and

$$\Delta U = .096 \text{ m/s}, \text{ S.D.} = 0.01 \text{ m/s}.$$

Thus, γ_T actually decreases 1% while ΔU increases significantly.

This result contradicts the earlier findings and suggests that the rather large discrepancies found in Table 2.1.2 are due to experimental error and do not signify changes of γ_T with changes of ambient temperature.

The seemingly large change in ΔU is not surprising since the bearings offer increased resistance toward motion as the temperature decreases. This effect does not seem of any importance, since the magnitude of errors introduced at wind speeds of 10 m/s is about 1%.

Definition of Symbols

a (m)	Length of blade segment chord
a_n (none)	Fourier coefficients
Az (degree)	Azimuth angle (variable)
Az_f (degree)	Azimuth angle (constant)
b_1 (m)	Blade thickness at propeller rod
b_2 (m)	Blade thickness at propeller tip
b_n (none)	Fourier coefficients
C_D (m^{-1})	Drag coefficient, 2-dimensional related to a
C_L (m^{-1})	Lift coefficient, 2-dimensional related to a
C_L^o $(rad \cdot m)^{-1}$	Lift coefficient per radian of incidence angle
$C.I._{.95}$	95% confidence interval
El (degree)	Elevation angle
i,j	Summing indices
I (kg m^2)	Moment of inertia of propeller
k (none)	γ_T/γ_R
L (m)	Distance constant
M (Nm)	Moment of forces
m,n	Summing indices
p (none)	Number not exceeding 0.1
p,g	Summing indices
$\bar{r}$ (m)	Radius vector. Coordinates (x, y, z), length r
R (m)	Radius of propeller
R_o (m)	Radius of propeller rod
S.D.	Standard deviation

Definition of Symbols cont'd

S.E.	Standard error
t (sec)	Time
T (sec)	Time scale
U_i (m/s)	Velocity vector in tensor notation. Components (U_1, U_2, U_3)
$\overline{U}$ (m/s)	Velocity vector with coordinates (U, V, W)
U_R (m/s)	Design velocity; unit velocity
V (m/s)	Magnitude of relative velocity, causing lift and drag on the propeller blade segments
α (rad)	Pitch angle
β (rad)	Pitch angle of relative velocity
γ_R (none)	Design pitchfactor: $U_R/R/\omega_R = \gamma_R$
γ_T (none)	Actual pitchfactor: $\gamma_T = k \cdot \gamma_R$
δ (none)	$\delta = r'/R \cdot 1/\gamma_R$, where r' has a certain value between 0 and R
ϵ (rad)	Incidence angle
η (degree)	Aspect angle of three dimensional propeller sensor
θ (rad)	Velocity attack angle
θ_o (rad)	Propeller threshold region: $\theta_o \leq \lvert\vartheta\rvert \leq 90^o$
ξ (degrees)	Angle between adjacent propeller axes
ρ_a (kg/m^3)	Air density
ρ_m (kg/m^3)	Density of propeller material
σ_Q^2	Variance of Q
ϕ (rad)	Angle describing propeller blade position: $\omega = d\phi/dt$
$\Delta\phi$ (rad)	Aspect angle of propeller blade

Definition of Symbols cont'd

ω (rad/sec)	Cyclic frequency $\omega = d\phi/dt$
ω_R (rad/sec)	Design frequency, unit frequency
ω_∞ (rad/sec)	Equilibrium cyclic frequency for axial flow
$\omega'(t)$ (none)	Cyclic frequency
$\omega'_o(t)$ (none)	Offset cyclic frequency
$\Omega(t)$ (none)	Cyclic frequency

A bar ($\bar{\ }$) on top of a letter denotes either a vector or a mean value. The context should indicate which meaning is used in each particular case.

In Chapter 1 vectors are denoted as tensors.

References

(1) Middleton, W.E.K. and Spilhaus, A.F., 1953: Meteorological Instruments, University of Toronto Press.

(2) Gill, G.C., Bradley, J. and Sela, J., 1967: The UVW-anemometer-an instrument to measure the three orthogonal wind vectors, separately and independently. Paper presented at the AMS Conference on Physical Process of the Lower Atmosphere, March 20-22, 1967, Ann Arbor, Michigan.

(3) R.M. Young Company
Product Bulletin
Traverse City, Michigan

(4) Durand, W.F., 1963: Aerodynamic Theory, Vol. IV, Dover Publications, Inc., New York.

(5) Goldstein, S., 1965: Modern Developments in Fluid Dynamics, Vol. II, Dover Publications, Inc., New York.

421/98 14:18